Communications Research Centre

A COMPARISON OF DIRECTION FINDING RESULTS FROM AN FFT PEAK IDENTIFICATION TECHNIQUE WITH THOSE FROM THE MUSIC ALGORITHM (U)

by

L.E. Montbriand

CRC REPORT NO. 1438

July 1991
Ottawa

Government of Canada
Department of Communications

Gouvernement du Canada
Ministère des Communications

COMMUNICATIONS RESEARCH CENTRE

DEPARTMENT OF COMMUNICATIONS
CANADA

A COMPARISON OF DIRECTION FINDING RESULTS FROM AN FFT PEAK IDENTIFICATION TECHNIQUE WITH THOSE FROM THE MUSIC ALGORITHM (U)

by

L.E. Montbriand

CRC REPORT NO. 1438

July 1991
Ottawa

A Comparison of Direction Finding Results From an FFT Peak Identification Technique With Those From the Music Algorithm

L.E. Montbriand

Abstract

A peak identification technique which uses the FFT algorithm is presented for unambiguously identifying up to three sources in signals received by the sampled aperture receiving array (SARA) of the Communications Research Centre. The technique involves removing phase rotations resulting from the FFT and the data configuration and interpreting this result as the direction cosine distribution of the received signal. The locations and amplitudes of all peaks for one array arm are matched with those in a master list for a single source in order to identify actual sources. The identification of actual sources was found to be subject to the limitations of the FFT in that there was an inherent bias for the secondary and tertiary sources to appear at the side-lobe positions of the strongest source. There appears to be a limit in the ratio of the magnitude of a weaker source to that of the strongest source, below which it becomes too difficult to reliably identify true sources. For the SARA array this ratio is near -10 dB.

Some of the data were also analyzed using the more complex MUSIC algorithm which yields a narrower directional peak for the sources than the FFT. For the SARA array, using ungroomed data, the largest side and grating lobes that the MUSIC algorithm produces are some 10 dB below the largest side and grating lobes that are produced using the FFT algorithm. Consequently the source-separation problem is less than that encountered using the FFT algorithm, but is not eliminated.

Comparaison, pour fins de radiogoniométrie, des résultats obtenus en utilisant la méthode d'identification des crêtes par TFR et des résultats obtenus à l'aide de l'algorithme MUSIC

L.E. Montbriand

Résumé

Ce rapport décrit une méthode d'identification des pointes qui utilise l'algorithme de la transformée de Fourier rapide (TFR) pour l'identification sans ambiguité d'un maximum de trois sources dans les signaux captés par le réseau de réception à ouverture échantillonnée (SARA) du Centre de recherches sur les communications. Cette méthode passe par (1) l'application de la transformée de Fourier rapide à une série de signaux captés sur l'une des deux sections du réseau récepteur, (2) l'élimination des rotations de phase dues à la TFR et à la configuration des données, (3) l'interprétation du résultat comme la distribution du cosinus de la direction du signal reçu, (4) la recherche des concordances entre les emplacements et amplitudes de toutes les pointes et ceux d'une liste maîtresse portant sur une source unique, (5) la reprise des étapes 1 à 4 avec les données de la seconde section du réseau et (6) la recherche des concordances entre la phase et l'amplitude des sources possibles sur une section et celles des sources possibles sur l'autre section. Les résultats indiquent que les limites de la TFR influent sur le processus d'indentification des sources possibles sur une section et celles des sources possibles sur l'autre section. Les résultats indiquent que les limites de la TFR influent sur le processus d'identification des sources, c'est-à-dire qu'il existe une tendance inhérente par laquelle les sources secondaires et tertiaires apparaissent aux positions des lobes latéraux de la source la plus intense. D'autre part, il semble exister un rapport limite entre l'amplitude de la source plus faible et celle de la source plus intense, au-dessous duquel il est difficile d'identifier avec fiabilité les autres sources réelles. Les pointes du lobe principal se trouvent entre les pointes de lobe latéral des pointes les plus intenses, tandis que les lobes latéraux d'autres sources ainsi que le bruit et le brouillage contribuent aussi au phénomène. Pour le réseau SARA, ce rapport est d'environ -10 d B.

On peut utiliser des données à équivalence temporelle pour obtenir des résultats directionnels correspondant à chaque balayage des récepteurs, tandis que le recours à des données rétrospectives sur ces balayages permet d'obtenir la fréquence Doppler des diverses sources. Ce paramètre peut servir à vérifier l'authenticité de certaines des plus faibles sources identifiées.

Certaines données ont été analysées au moyen de l'algorithme MUSIC. La pointe directionnelle des sources est plus étroite avec cet algorithme qu'avec la transformé de Fourier rapide. Dans le cas du réseau SARA avec donnés non traités, les plus gros lobes latéraux et lobes de diffraction produits par l'algorithme MUSIC sont inférieurs de 10 dB aux plus gros lobes latéraux et lobes de diffraction produits par l'algorithme TFR. Par conséquent, le problème de séparation des sources est moins crucial que dans le cas de l'algorithme TFR, sans disparaître tout à fait. L'algorithme MUSIC n'est pas aussi facile d'utilisation et est beaucoup plus lent que les méthodes conventionnelles, y compris la méthode d'identification des pointes décrite plus haut .

Executive Summary

A peak identification technique is presented which uses the FFT algorithm for unambiguously identifying up to three sources in signals received by the sampled aperture receiving array (SARA) of the Communications Research Centre. The technique involves (1) performing an FFT on a set of signals received by one of the two arms of the receiving array, (2) removing phase rotations resulting from the FFT and the data configuration, (3) interpreting this result as the direction cosine distribution of the received signal, (4) matching the locations and the amplitudes of all peaks with those in a master list for a single source, (5) repeating steps 1 to 4 with the second-arm data and (6) matching the phase and amplitude of potential sources on one arm to the phase and amplitude of potential sources on the other arm. The identification of the sources was found to be subject to the limitations of the FFT in that there was an inherent bias for the secondary and tertiary sources to appear at the side-lobe positions of the strongest source. There appears to be a limiting ratio of the magnitude of a weaker source to that of the strongest source, below which it becomes too difficult to reliably identify other true sources. Their main-lobe peaks fall between the side-lobe peaks of the strongest peaks, but also present are contributions from side lobes of other sources and from noise and interference. For the SARA array this ratio is near -10 dB.

Time equivalent data can be used to determine directional results for each scan of the receivers and based on a time history of such scans it is possible to determine the Doppler frequency of the different sources. This information can be used to verify the authenticity of some of the weaker sources identified.

Some of the data were also analyzed using the MUSIC algorithm. The MUSIC algorithm yields a narrower directional peak for the sources than the FFT. For the SARA array, using ungroomed data, the largest side and grating lobes that the MUSIC algorithm produces are some 10 dB below the largest side and grating lobes that are produced using the FFT algorithm. Consequently the source-separation problem is reduced relative to that encountered with the FFT algorithm, but is not eliminated. The MUSIC algorithm is not as simple to use and is much slower than conventional techniques, including the peak identification technique described above.

TABLE OF CONTENTS

TABLE OF FIGURES

1. Introduction

The fast Fourier transform (FFT) is widely used today to replace the slower Fourier transform. The discrete-time version, or DFT, has been used by many in the past 15 years for processing data recorded by the sampled aperture receiving array (SARA) at the Communications Research Centre (CRC), e.g., Rice (1973), Rice and Winacott (1977), Montbriand (1981). The potential and limitations of using the DFT for separating two or more signals received by the SARA array had not been adequately investigated in the past, and such a study was made a part of a cooperative study CRC participated in with the Naval Oceans Systems Center (NOSC). This report presents the method and results of CRC's part of that study.

Section 2 briefly describes the DFT procedure, including the phase rotations that are present in the results as a result of the DFT itself, as well as phase rotations which are introduced by the positioning of the data samples in the data array used by the DFT when the data sample length is shorter than the data array length. It is shown that removing these phase rotations is the key to matching sources identified on one array arm with the same source identifiable on the other arm. Directional aliasing is discussed, and it is shown that the uneven spacing of the elements of the SARA array makes it possible to unambiguously resolve directionally aliased results. Section 3 examines the case where the data samples are not evenly spaced. It is shown that it is usually better to insert zeros for missing data samples, but that under certain circumstances it is better to use linearly interpolated results for the missing samples. Section 4 describes a Peak Identification (PI) technique that was developed and the DOPFUR and TIMFUR analysis programs that used this technique for uniquely identifying two, three and in rare cases four sources. Section 5 presents simulation results of the resolution study using a special version of DOPFUR called RESL. Section 6 presents experimental results on Doppler-frequency-separated data using the DOPFUR program and Section 7 presents experimental results using the TIMFUR program on raw data which had been corrected into an equivalent time sequence. Section 8 in conjunction with Appendix A details the program TMUSIC for processing data from the SARA array using the MUSIC algorithm. Some of the results obtained from this program are presented in Section 9 for simulated and experimental data.

2. Theoretical

2.1 Discrete Fourier Transform

The DFT is summarized as follows: if x_n is the n-th of N signal samples spaced in time or position then X_k, the k-th of N unambiguous frequency components spaced in frequency or direction-cosine is given by:

$$X_k = \sum_{n=0}^{N-1} x_n \exp[(-j2\pi kn)/N] \qquad (1)$$

where k has the values $0, \pm 1, \pm 2, \ldots \pm(N-1)/2$ and $-N/2$.

2.2 Phase Rotations in DFT Resulting From Signal and DFT

The DFT converts the sample data into frequency components, and the left side of equation (1) gives the phase and amplitude of each frequency component. The phase is made up of two components, one due to the signal, which is described below, and the other due to the DFT. This latter component can be seen in terms of each of the X_k frequency components and the phase they would have at the centre position of the data sample. For $k = \pm 1$ (see Figure 1) the phase at the first and last + 1 position is 0°; and at the centre 180°. For $k = \pm 2$ the centre phase is 0°; the centre phase thus increments 180° with each increment of k. This centre phase rotation is due to the DFT and can be removed by multiplying each component in (1) by $\exp[j\pi k]$. The expression for X_k becomes:

$$X'_k = \exp[j\pi k]X_k \qquad (2)$$

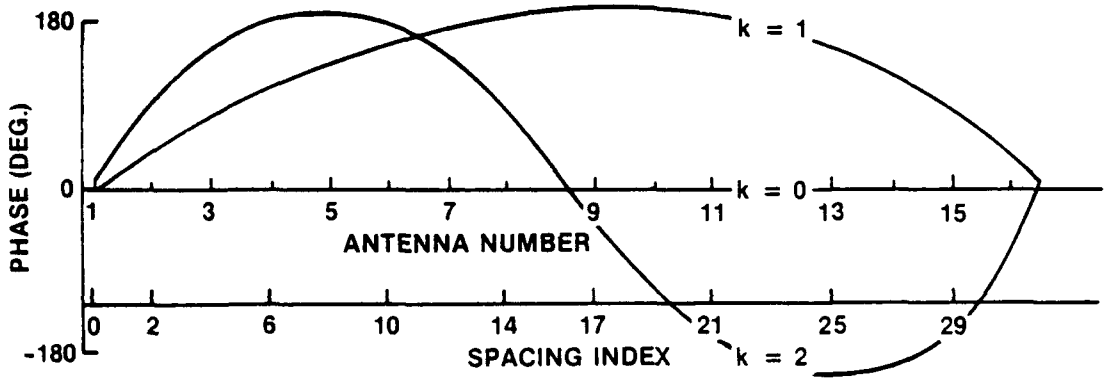

Figure 1. Variation of phase over data set for Fourier indices k=0,1 and 2.

The phase remaining is that due to the signal. The resulting responses X'_k due to the signal can be understood by noting that the variation of the magnitude and phase of the X'_k values with k will be the same as the directional response of a uniformly weighted linear antenna array. In both cases there is a main lobe, side lobes and nulls. In the case of a linear array, an X'_k value actually corresponds to the response of an array steered in a direction given by k (as indicated in Section 2.5). For a steering index k_j, the main lobe (in k-space) falls on k_j and the nulls and sidelobes are displaced from k_j by fixed amounts which do not depend on k_j. A signal from one direction thus has an entirely predictable set of responses X'_k once its centre direction k_j is defined. The main lobe has a phase Φ and the side lobes a phase of Φ or $\Phi+\pi$, and this phase as indicated above corresponds to that at the centre of the data sample or the antenna array. When more than one source is present, the amplitude and phase at each index k will correspond to the vector sum of the components from each source. Removing the phase rotation due to the DFT allows one to examine this amplitude and phase structure and is a key to matching a source identifiable on one array arm with the same source identifiable on the other arm, since both arms have the center position in common.

2.3 Phase Rotation Due to Number of Samples Shorter Than FFT Data Array Length

If the number of data samples is η and is less than the FFT data array length N the actual summation is over η rather than N. The 180° phase rotation between frequency bins is reduced to $180.\eta/N$ and equation (1) becomes:

$$X'_k = \exp\,[j\pi k\eta/N]X_k \tag{3}$$

By multiplying each frequency component by $\exp[j\pi k\eta/N]$ the phase rotation due to the difference in the sample length and the FFT array length is removed. (For the SARA array used, which is described later, $N = 2048$ was used and for the short arm, which contains 16 elements spread over $\eta = 31$ inter-element spaces of 7.62 m, the phase rotation is 2.72° between frequency bins. For the long arm, which contains 42 elements spread over $\eta = 155$ inter-element spaces of 7.62 m, the phase rotation is 13.62° between frequency bins.)

2.4 Phase Rotation Due to Placement of Samples in FFT Data Array

If the number of samples η is less than N and the η values of x are positioned in the N-point data array starting at $n + \Delta$ where Δ is the number of zero terms preceding the first non-zero data value, then the signal in frequency bin k is:

$$X_{k\Delta} = \sum_{n=0}^{\Delta+\eta-1} x_n \exp[(-j2\pi k(n+\Delta))/N] \tag{4}$$

which can be expressed as

$$X_{k\Delta} = \exp[(-j\,2\pi k\Delta)/N]X_k \tag{5}$$

The exponential part of the expression represents the phase rotation due to the position of the samples in the data array to be processed by the FFT. This phase rotation, ϕ at the frequency bin k, where $k = 0, \pm1, \pm2$, etc. is:

$$\phi = arctan[-tan(2\pi k\Delta/N)] = -2\pi k\Delta/N \tag{6}$$

This phase rotation due to the positioning of the samples in the data array can be eliminated by stacking the non-zero samples at the beginning of the data array.

2.5 Cone Angle

The cone angle is defined as the angle between the array arm and the direction of the incoming signal. This cone angle can be related to spatial frequencies by converting to direction cosine index (I) by:

$$I = fUN \sin\theta / c \tag{7}$$

where

f = radio frequency (MHz)

U = element of unit spacing (7.62 meters for the SARA array)

N = number of elements in FFT array (a power of 2)

θ = cone angle of source

c = velocity of light (km/s)

The direction cosine index is exactly the same as the frequency index k in equation (1) and has the values I = 0, ±1, ±2,...±(N-1)/2, -N/2 where I = 0 corresponds to the boresight direction, θ = 0 °, orthogonal to the array line.

2.6 Grating Lobes

A grating lobe, or ambiguous direction-of-arrival result is termed direction aliasing and occurs when the antenna spacing for the radio frequency used results in more then one possible solution for the DOA of an incoming signal. When the array is steered to a cone angle of 0°, the grating lobe has a cone angle given by

$$\sin(\theta_g) = M\, C / (f\, n\, U) \tag{8}$$

where

θ_g = cone angle of the wavefront at a grating lobe

M = grating lobe order, 0, 1, 2, ...

n = number of unit spacings U between adjacent antennas

There is a different θ_g for each nU (and value of M), and the importance of each depends on how many times the spacing nU occurs in the array.

2.7 The SARA Array and the Antenna Patterns of its Arms

The SARA array used in the Texas to Ottawa test is illustrated in Figure 2. It is composed of 42 elements in a north-west to south-east arm and 16 elements in an orthogonal south-west to north-east arm. The short arm has 14 inter-element spacings of 15.24 m and one of 22.86 m. On the long arm there are 16 inter-element spaces of 15.24 m, one of 22.86 m and 26 spaces of 38.10 m. In both arms the 22.86 m inter-element space is located at the centre. Tests can be performed using groupings of elements within each arm; this work is concerned with the 42 by 16 and the 16 by 16 (inner) element arrays.

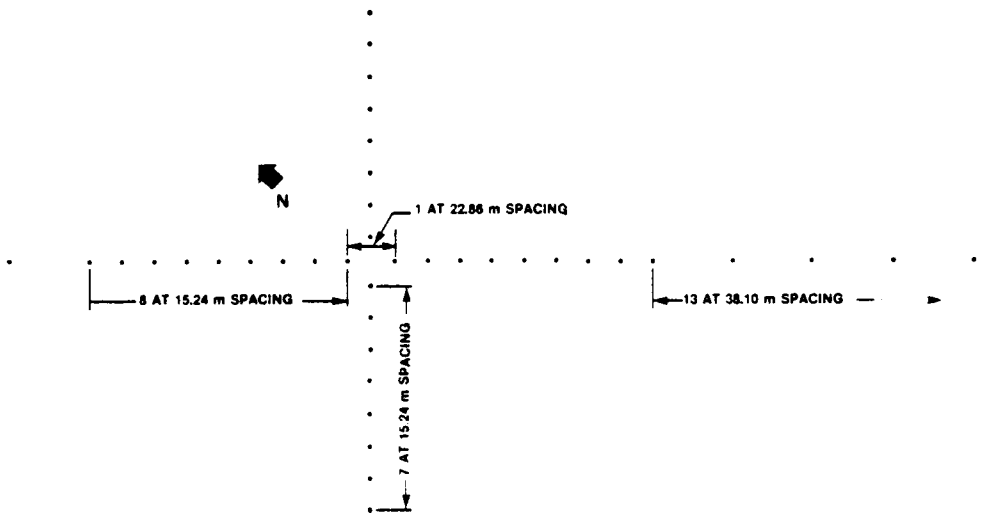

Figure 2. SARA array configuration. Minimum spacing utilized was 15.24 m with 22.86 m at the centre.

For a single source near endfire of the short arm the antenna or radiation pattern for the short 16-element array is shown in Figure 3. Each of the peaks corresponds to a main, grating or side lobe and has a phase, relative to that of the main lobe, of either 0°or 180°. As a means of illustrating both amplitude and peak phase in one graph, all peaks with 180° phase were replotted in Figure 4 as having negative amplitudes. Figure 5 shows a similarly plotted pattern for the long arm. Again, the magnitudes are coded positive and negative, with positive values indicating the phase of the main lobe (Φ) which is near the direction cosine index -747 in Figure 4 and -87 in Figure 5. The negative values indicate a phase Φ + 180°.

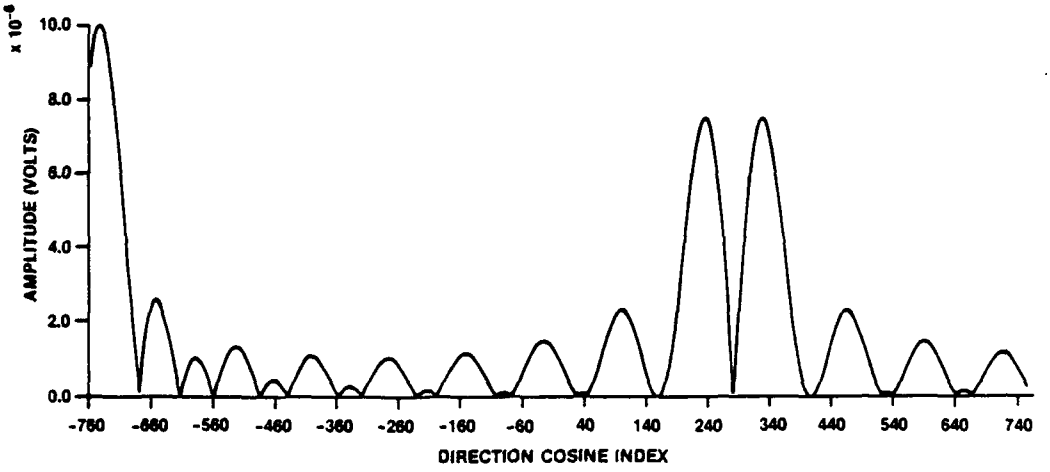

Figure 3. Directional response of short arm.

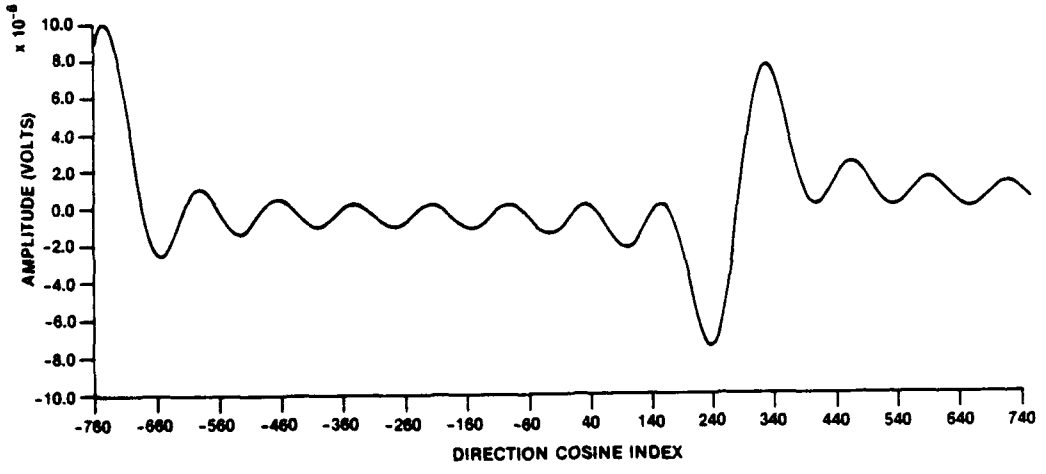

Figure 4. Phase coded directional response of short arm. Positive amplitudes are for 0.0° and negative amplitudes are for 180.0°.

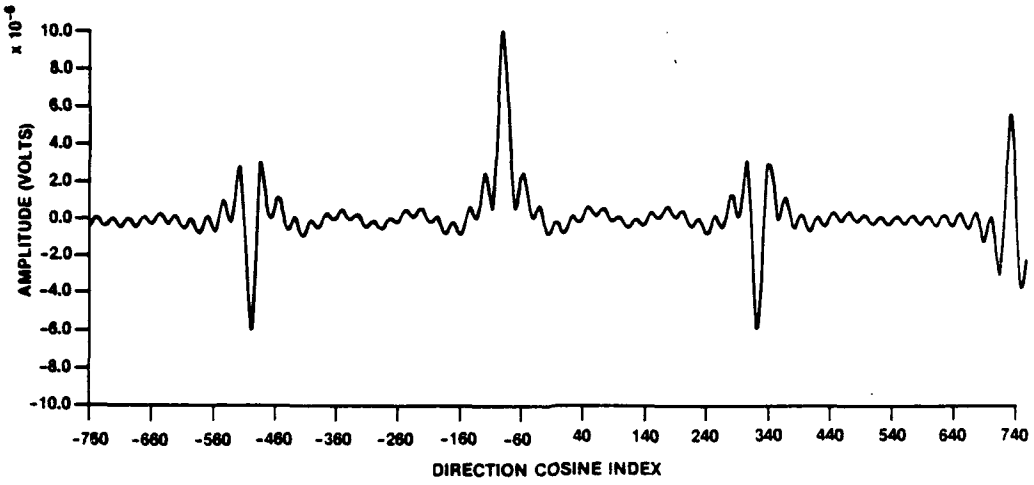

Figure 5. Phase coded directional response of long arm. Positive amplitudes are for 0.0° and negative amplitudes are for 180.0°.

2.8 Phase at the Centre of the Array Arm

The phase of the main lobe is Φ and, as indicated earlier, this is the signal phase at the centre of the array arm. When two sources are present and located at different sky locations (elevation and bearing), each source will have a relative directional distribution which has the same shape but differs in the absolute locations of the main and other lobes and in the amplitudes of these lobes. The combined directional distribution is the vectorial sum of the two directional distributions. There will be two main lobes and they will have phases near Φ_1, the phase of the first source, and Φ_2, the phase of the second source. If the two main lobes are not separable on an arm, the combined main lobe has a phase between Φ_1 and Φ_2.

2.9 Capability of Resolving Direction Aliasing if Data Recorded by Unevenly Spaced Array

One of the problems encountered by the SARA array is that the most commonly used narrowest spacing between elements, $2U$ or 15.24 m, is large enough for grating lobes to occur. For frequencies slightly above 19.67 MHz a source at a cone angle of 90° will also appear at a cone angle just above 0° and just less than 180°. The next shortest inter-element space is 22.86 m. Its grating lobe structure interacts with the first grating lobe for the 15.24 m spacing to produce the modulated peaks in Figure 4 centered at the direction cosine index (DCI) = +282. The two peaks have equal powers which are 2.5 dB smaller than that of the main lobe, and have opposite phases. The long arm has inter-element spaces of 15.24, 22.86 and 38.10 m and these produce the grating lobes in Figure 5 at DCI = -497, 322, and 728 with magnitudes 3.1, 3.1 and 3.2 dB, respectively, below that of the main lobe.

Thus, from these figures it is seen that the signals and phases at the grating lobes for an unevenly spaced array are not duplicates of the main lobe. They have their own unique signature of direction cosine index, phase and magnitude which makes it possible to positively identify them as grating lobes.

Directional aliasing for the SARA array will occur for all inter-element spacings when the radio frequency f is greater than 19.67 MHz. For f = 19.87 MHz and M = 1 at DCI = 1024 the cone angle is 0° and there is no aliasing but for f = 24.00 MHz and M = 1 at DCI = 1024 the cone angle is 34.95° and aliasing occurs over cone angles 0 to 34.95°. Stated in terms of the DCI, aliasing occurs when the direction cosine index I as defined by equation (7) for a frequency f increases above N, the number of elements, as the cone angle θ increases. When this happens, the magnitudes at DCI ≥ -1024 are repeated at DCI ≥ +1024 and the magnitudes at DCI ≤ +1024 are repeated at DCI ≤ -1024. This is shown by the upper curves in Figure 6 which is an extended reproduction of Figure 3. When phase is considered also, we note that the distribution from DCI = -1024, -1023,...1024 cannot be merely repeated at +1024; all the aliased points must have 180° added to their phase. In this way the phase is continuous at the aliased points. The same applies when the points ending at +1024 are repeated at -1024. Note that the aliased main lobe has a phase which is 180° different from that of the principal main lobe. The same principle applies to the long arm. Thus, by comparing the phases on each arm, the aliased main lobe can be identified and eliminated.

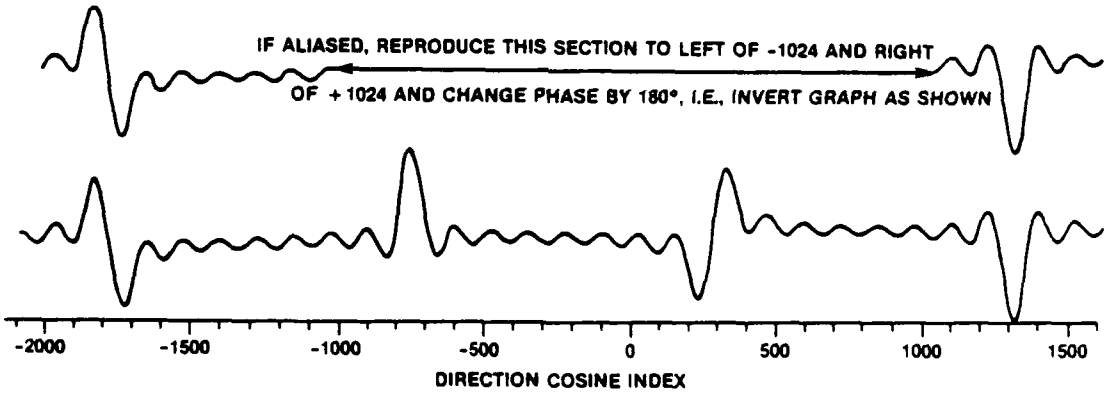

Figure 6. Phase coded directional response of short arm illustrating aliasing.

3. Unevenly Spaced Samples

3.1 Value to Use For Missing Samples

Replacing the missing samples or, in this case signals at missing antennas, with zeros is a common practice and has been regularly used for processing signals recorded by the SARA array. When such a data sample is processed with an FFT, and the signal is from an isolated source, the resultant directional distribution corresponds to the radiation pattern of the sampling array with the elements phased in the direction of the source. Figure 7 illustrates a portion of the radiation pattern of the long 1181.1 m arm of the SARA array for four array configurations (i) 155 inter-element spacings of 7.62 m, (ii) a thinned array with 35 spacings of 7.62 m and 24 spacings of 38.10 m, (iii) 32 spacings of 7.62 m, 1 spacing of 22.86 m and 24 spacings at 38.10 m and (iv) 16 spacings of 15.24 m, one of 22.86 m and 24 spacings of 38.10 m. As can be seen, each configuration has its own antenna pattern.

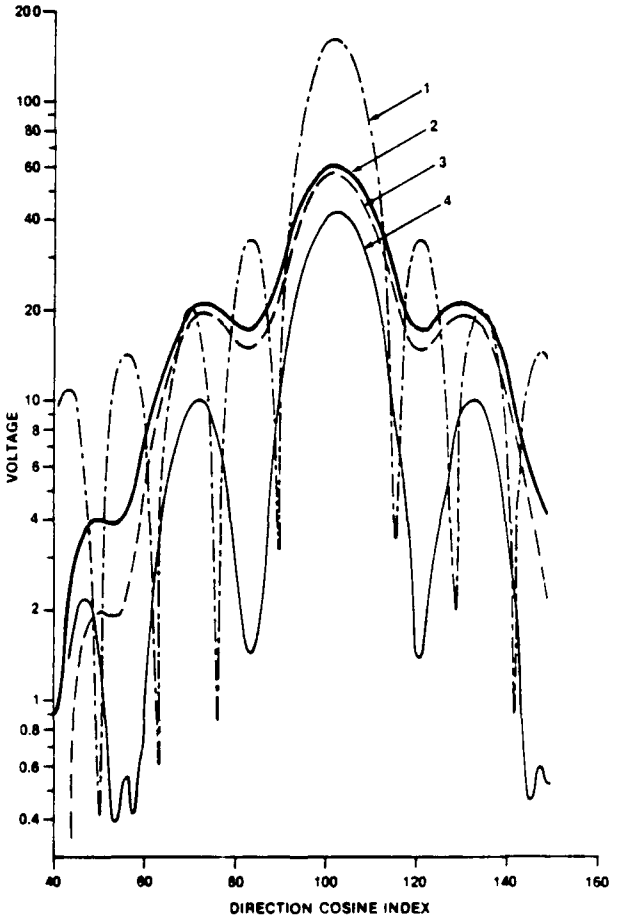

Figure 7. Portion of directional distribution for 4 configurations of 1181-m-long arm. Legend: 1- 155 spaces at 7.62 m; 2- 35 spaces at 7.62 m and 24 spaces at 38.10 m; 3- 32 spaces at 7.62 m, 1 space at 22.86 m and 24 spaces at 38.10 m; 4- 16 spaces at 15.24 m, 1 space at 22.86 m and 24 spaces at 38.10 m.

3.2 The Effect of Replacing Signals at Missing Antennas With Interpolated Values

If signals at missing antenna positions are replaced with interpolated values, the effect for a very restricted range of radio frequencies and source directions as indicated below, will be to add new antennas and to change the radiation pattern. If all the missing antenna positions are suitably replaced, the radiation pattern becomes the same as that of a filled-in array. If this change in the antenna pattern is of no consequence, it is safer to replace missing samples with zeros so as to eliminate any possibility that the interpolation could produce any deterioration in the directional distribution because of aliasing. This is discussed below.

In order to understand what happens when interpolation is used, it is useful to regard the signals at the antenna elements as a short sequence of unevenly spaced time samples, with the unit of time corresponding to units of the inter-element spacing. For such a "time" sample, aliasing will occur if $|f| \geq f_s/2$ where f is the radio frequency and $f_s = 1/T_s$ where T_s is the time between samples. There will be *no aliasing* if $T > 2T_s$ where T is the period of the radio frequency. Now consider the irregularly spaced samples shown in Figure 8 where the filled dots correspond to the samples and the "X"s the interpolated values. This sequence represents a portion of the 236-m short array arm, and for this study includes the single $T_s = 6$ units of 3.81 m and some of the 14 cases with $T_s = 4$ units of 3.81 m. For this sequence there is no aliasing as long as $T > 12$ units of 3.81 m. This is illustrated in Figure 9 where each curve presents a portion of the post-FFT frequency spectra (or directional distribution) for the case where the signals at the missing antennas were estimated by using a crude linear interpolation between samples. For $T \geq 12$ the spectra were identical. For $T = 11$, 10, and 9, as the aliasing for the $T_s = 6$ interval becomes greater, there is a noticeable deterioration in the lobe structure of the spectrum. At $T = 8$ the main lobe amplitude decreases, and at $T = 7$ the lobe structure in the spectrum vanishes. At $T = 7$ the frequency was greater than the Nyquist frequency $f_s/2$ of the largest inter-element spacing, and the interpolation failed and could not be used to successfully replace missing samples. However, as we shall now see, for a restricted set a directions, interpolation can still be used.

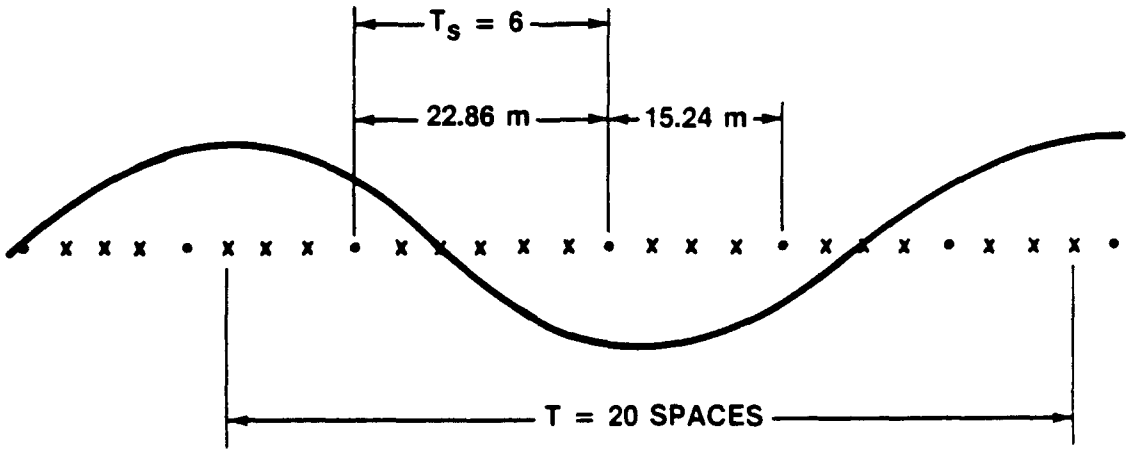

Figure 8. End-fire wave along centre portion of array arm.

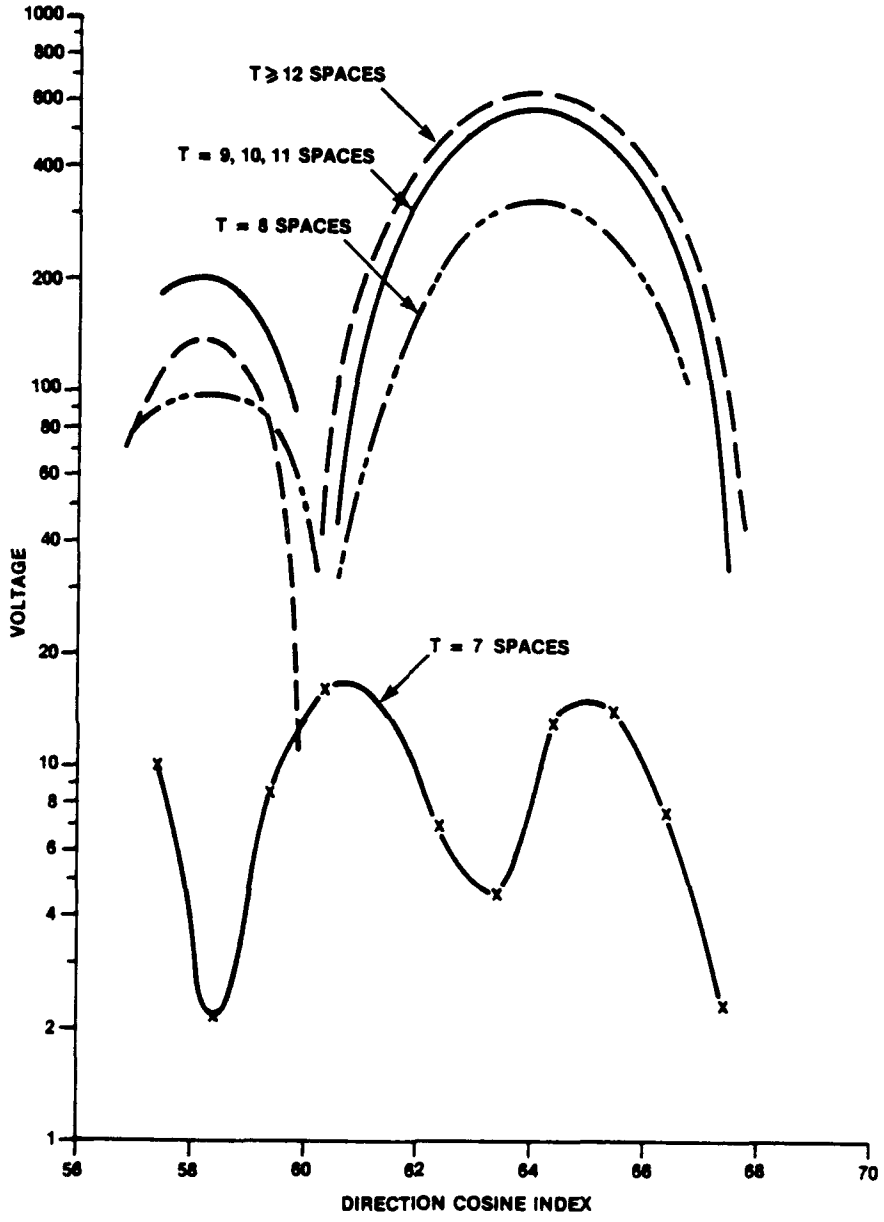

Figure 9. Portion of directional response of short arm for indicated T and use of interpolated values at missing points.

Let us now return to the samples as signals from an unevenly spaced array. The wave shown in Figure 8 and the waves discussed to this point are for a source in the end-fire position with wavefronts perpendicular to the array arm. The wave shown is for a radio frequency f = 3.94 MHz with a wavelength λ_{ef} along the array arm of 20 units of 3.81 m. Signals received by the SARA array are normally other than end-fire, arriving at an angle θ to the array arm. For such a signal $\lambda_{ef} = \lambda / \cos\theta$ where λ is the wavelength of the radio frequency at the angle θ and $\lambda = 299.7925/f$ where f is the radio frequency in MHz. As indicated above, there is no aliasing and no deterioration of the directional distribution as long as $T > 2T_S$. Substituting in this expression $T = \lambda_{ef}$ and T_S = d, where d is the inter-element space, replacing λ_{ef} and rearranging, one obtains for the condition of no aliasing,

$$\cos\theta < 299.7925/2\,df \qquad (9)$$

The angle θ is thus required to be greater than *arc cos* (299.7925/2 df), and values of this angle for the three inter-element spacings of the long arm of the SARA array are listed in Table I for selected frequencies. In summary, interpolation can only be used if the source angle lies between the 90 degree angle and that listed in the table.

Table I

Tabulations of Minimum Angle (degrees) to the Array Arm Direction For Which Interpolated Values Can be Used For Missing Antennas of the SARA Array

Spacing d(m)	No. of Occurences	Frequency f(MHz)								
		7	10	13	16	19	22	25	28	31
38.10	24	55.8	66.8	72.4	75.8	78.1	79.7	81.0	81.9	82.7
22.86	1	20.5	49.0	59.7	65.8	69.8	72.7	74.8	76.5	77.8
15.24	16	00.0	10.4	40.8	52.1	58.8	63.4	66.8	69.4	71.5

As a means of demonstrating the effect of a linear interpolation, consider a radio frequency of 10 MHz and three sources located at 80°, 30° and 5° to the long array arm. For the source at 80° to the long arm, interpolation over even the largest spacing, 38.10 m will not result in aliasing. However, for the source at 30° there will be aliasing in both the 24 cases of a 38.1 m inter-element space and the single case of an inter-element space of 22.86 m and this aliasing will result in very serious deterioration in the resultant directional distribution. For the source at 5° there will be aliasing for all inter-element spacings and the aliasing will result in catastrophic deterioration of the directional distribution. The combined directional distribution of the three sources will be seriously affected. A combined directional distribution on the orthogonal short arm will also be affected but in a different sense. One could not use such a directional distribution to locate even one of these sources. For cases such as this, zeros would have to be used for signals at the missing antennas.

If a more precise interpolation algorithm is used the directional distribution curves would be better. Such an algorithm could use a combination of zero filling for the largest inter-element spaces and interpolation for the smaller spaces. The most mathematically sound procedure is to always replace the missing samples with zeros.

4. DOPFUR and TIMFUR Analysis Programs Using the PI Technique

The programs DOPFUR and TIMFUR, which process data using a fast Fourier transform, are essentially identical except that the former uses data that has been preprocessed into 256 separate Doppler frequencies and the latter uses data that has been preprocessed into 256 equivalent time samples. The intent of both programs is to perform second-stage processing using an FFT to convert the received signal into a directional distribution, and to utilize the Peak Identification (PI) technique described below to identify and classify each of the various peaks in the distribution as corresponding to a particular type of pattern lobe. This is done for the signals on each arm. Peaks which are identified as main lobes on one arm and which correspond to peaks identified as main lobes on the other arm are referred to as matched peaks. The sky location of the intersecting cone angles of these matched peaks indicate the elevation and bearing of the incoming signal.

The main part of the PI technique is the classification of each of the identified peaks according to lobe type by matching these peaks to the various lobes given in a master list. A list of the 28 most intense lobes for the long arm and the 20 most intense lobes for the short arm for a single source is presented in Tables II and III. In these tables the main lobe, which corresponds to the strongest peak, is given a relative direction cosine index (DCI) of 0.0, and a relative power in dB of 0.00. In the heading 'Lobe', M represents a main lobe, G a grating lobe and S a side lobe. U is used to indicate an unidentified peak. For each peak the DCI and relative power are relative to the main lobe. These tables are for an FFT array size of 2048 points.

Table II

Peak Positions and Magnitudes of the 28 Largest Pattern Lobes of Arm 1

DCI	dB	Lobe	DCI	dB	Lobe	DCI	dB	Lobe	DCI	dB	Lobe
0	0.00	M	31	-14.53	S	71	-16.77	S	366	-16.99	S
392	-9.52	S	410	-3.12	G	428	-10.38	S	776	-16.48	S
802	-8.52	S	819	-4.53	G	838	-7.12	S	863	-12.77	S
970	-11.71	S	991	-10.78	S	1059	-10.78	S	1079	-11.71	S
1186	-12.76	S	1211	-7.11	S	1229	-4.52	G	1247	-8.69	S
1273	-16.46	S	1621	-10.38	S	1639	-3.30	G	1657	-9.65	S
1698	-16.98	S	1977	-16.17	S	2017	-14.53	S	2048	0.00	M

Table III

Peak Positions and Magnitudes of the 20 Largest Pattern Lobes of Arm 2

DCO	dB	Lobe	DCI	dB	Lobe	DCI	dB	Lobe	DCI	dB	Lobe
0	0.00	M	89	-11.75	S	153	-19.56	S	216	-17.43	S
341	-19.31	S	466	-19.62	S	591	-18.79	S	716	-16.75	S
842	-12.81	S	978	-2.51	G	1071	-2.51	G	1207	-12.81	S
1333	-16.75	S	1458	-18.79	S	1583	-19.62	S	1708	-19.31	S
1833	-17.43	S	1896	-19.56	S	1959	-11.75	S	2048	0.00	M

The above lobes other than the main lobe are the grating lobes for the narrowest inter-element spacing, 15.24 m, and all the strongest side lobes. A test was carried out to determine the optimum FFT lengths for the two arms; they were found to be 512 points for the long arm and 128 points for the short arm. These lengths were considered optimum because identical elevations and bearings could be obtained using these or larger FFT lengths, but the computation time was much shorter using the smaller FFT arrays. The DCI values listed in Tables II and III were normalized to the 512 and 128 points in the programs.

When only one radio source is present, the FFT yields a directional distribution having only the directional peaks listed in Table II or Table III. When several sources are present, each has an identical directional distribution and at each DCI the contributions of each source are vectorially summed. During such conditions the locations of some of the peaks and their maximum power no longer correspond perfectly to those in the tables.

Listed below, and described in conjunction with the parameters indicated in Figure 10 are the steps used in the programs DOPFUR and TIMFUR for identifying a source or sources. They are in two stages.

4.1 Stage I of PI Technique. Identification and Coding of Peaks

1. *Lower limit of power of peaks*: Weak sources were difficult to unambiguously identify because the difference between the actual and theoretical array patterns was used to identify the presence of potential auxiliary sources. The signals are complex rather than real so the pattern magnitudes could not be merely subtracted to identify weaker peaks. It was necessary to set a limit in peak power (in dB) below that of the largest peak, below which peaks were deemed to be too weak to be confidently identified as potential sources. A 9.1-dB limit was found to be optimum; use of this limit, as can be determined from Tables II and III would result in about ten peaks on the long arm and about four peaks on the short arm when only a single source was present. If more peaks were identified, the data set was suspect and treated as indicated in Sec. 4.2 (7).

2. *Determine precise* DCI: Precise values of the relative DCI, maximum amplitude and the phase (with all phase rotations removed) of each peak were obtained by employing a five-point parabolic fit to the data.

3. *Position matching and position code:* The largest peak was taken as the main lobe. The precise relative position of each peak to this main lobe was determined. The position of each peak was then matched to the position of each peak in the reference list. The position discrepancy between the experimental peaks and the theoretical ones in the list was investigated; and it was found that a position uncertainty of less than ±1.5 units for both the 512-point FFT of the long arm and the 128-point FFT of the short arm was satisfactory for locating peaks. A peak within such position uncertainties was assigned a *position* code corresponding to the type of lobe it matched, i.e. M, G or S, and failing that a U.

4. *Power matching and power code:* For the lobe found in (3) the experimental power relative to that of the main lobe was compared to the corresponding value in the master list. How much of a power uncertainty could be allowed was investigated and a power uncertainty of ±1.25 dB for a grating lobe and ±2.5 dB for a side lobe were found to be satisfactory for matching peak powers. A peak within such power limits was assigned the *power* code of the same type of lobe found in (3.)

4.2 Stage II of PI Technique. Matching a Peak on the Long Arm to a Peak on the Short Arm

The following steps, 1 through 7, in the sequence listed was found to be successful for matching peaks and thus identifying sources.

1. *Matched centre phases:* Each peak found in the long arm data was matched to each peak found in the short arm data, and potentially a peak on one arm could match several peaks on the other arm. If the phase of a peak on the long arm (evaluated, as indicated in Section 2.5 as the phase at the centre of the array arm) differed from the phase of a peak on the short arm by more than 45 degrees the peaks were considered as non-matching. (The 45 degrees phase difference limit is somewhat arbitrary. However, in a separate study it was found that both position (Sec. 4.1.3) and power (Sec. 4.1.4) codes were usually satisfied if this difference was less than 45 degrees, but only occasionally if the phase difference was more than 45 degrees.) Consequently, if the phase difference was less than 45 degrees, a *possible* match of peaks was considered to be found.

Peak pairs satisfying this step were then scrutinized by Steps 2 and 3.

2. *Main lobes match:* If the peak coding for *position* on both arms was that of the main (M) lobe, a peak match was unambiguously found and the main source was identified.

3. *Grating lobes and side lobes match:* If the peak coding on either arm was a grating (G) lobe or a side (S) lobe for *both position and power*, no source could be identified as any match would not be that of a source but that of auxiliary lobe structures.

4. *Single peak for several sources:* At this stage of source identification most peak combinations would have been eliminated. Of those not, there were cases of one, two or three peaks on the long arm which matched the same single peak on the short arm. For such cases it was realized that the single overlapping or combined peak on the short arm had a phase and amplitude which was the vector combination of the components of several peaks and as such its combined amplitude and phase would not match perfectly any of the peaks on the long arm. All such peaks on the long arm were taken as possible matches to the single peak on the long arm and all such combinations were taken as possible sources. Their identification as sources was dealt with as described in (5).

5. *Power difference on two arms:* If the power of a peak on one arm greatly exceeded the power of a peak on the other arm, the peaks were considered as non-matched. A cutoff power ratio between the two peaks was used. A study of this problem indicated that when the ratio of the two peaks was large the weak peak was usually ambiguous on both arms whereas when the ratio was small the weaker peak was usually unambiguously present on the one arm in spite of being usually swamped by the large peak on the other arm. A cutoff power ratio of 10 dB between the two peaks was used. Peak combinations which had satisfied all previous conditions, and for which the power difference was less than 10 dB, were considered as matching peaks corresponding to true sources.

6. *Limit of number of sources identifiable:* Based on an examination of a large number of results at this stage of peak matching it was found that the maximum number of sources that could be reliably identified was near three. For cases when the number of sources identified was greater than three, the extras were considered to have possibly resulted from the vector sum of side lobes and grating lobes of the 3 main sources and a possible main lobe of another source. In such cases the DCI positions and powers of these peaks may have been sufficiently altered to enable them to satisfy the above steps to be identified as a source. Therefore it was decided that when more than three sources were identified, none of the sources would be considered as positively identified. (Armed with a time history of sources it was sometimes possible to positively identify up to four sources even if four or five possible sources were identified. Only rarely could a fourth source be accepted as a true source.)

7. *Limit of number of peaks identified:* Normally 10 peaks, made up of the main, grating and side lobes of the sources were identified in the directional distribution of the long arm and 4 in that of the short arm. When the number of peaks exceeded 15 and 7 respectively, it was recognized that many sources were present, some multipath and some interference. At such times a number of possible sources, ray paths or unidentified matching peaks ranging from 1 to 10 were identifiable. Because almost all were dubious, it was decided that if more than 15 and 7 peaks were found on the long and short arms, none of the possible sources would be treated as positively identified. Armed with a time history of accepted sources it was possible to positively identify one or two sources at the time of a brief but severe burst of interference or noise, even when a few more than 15 and 7 peaks were identified. At other times such identification was impossible.

4.3 Additional Remarks

1. When multipath is present and the sources are nearly coincident, the largest peak merely represents the mean position of the multiple sources. In this case there are substantial errors in the bearings and elevations of the sources. If precise sky positions are required, superresolution techniques would need to be employed for such cases.

2. The different limiting parameters that were used, and are indicated in Figure 10, are somewhat arbitrary. They are the 9.1-dB difference between the strongest peak and the weakest peak confidently identified as a possible source (Sec. 4.1 (1)), the 1.5 DCI units as the limit in position uncertainty of a peak (Sec. 4.1 (3)), the 2.5- and 1.25-dB peak power uncertainty (Sec. 4.1 (4)), the 45-degree phase matching uncertainty (Sec. 4.2 (1)) and the 10-dB power difference limit between matching peaks on the two arms (Sec. 4.2 (4)). The upper limits of three sources (Sec. 4.2 (6)) and the 15 and 7 peaks (Sec. 4.2 (7)) are also somewhat arbitrary. Use of values other than those above, if only one source is present, will not alter the results, but if multiple sources are present, they could change the number of peaks identified on each arm and the number of possible sources identified.

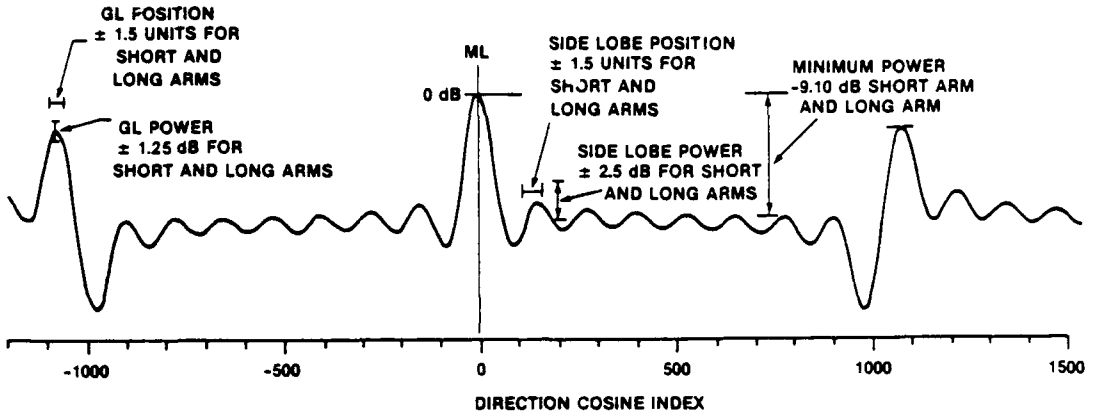

Figure 10. Illustration of some of criteria for identifying sources.

3. When the geographical location of a signal source is known, a range of acceptable elevations and bearings can be assumed for the arrival direction. Care must be exercised with such an assumption. What may fall within this allowed range of elevations and bearings may be the grating lobe and side lobes of an interfering signal whose main lobe may be located elsewhere.

5. Theoretical Study of Resolving Two Sources Using an FFT

5.1 Resolving Limit of the Two Arms

The main factor which affects the separate identification of two sources when their received signals are processed by an FFT is the width of the main lobe. This width dictates the resolution limit. Based on a 2048-point FFT, the -3-dB width is 12.4 DCI units wide for the 42-element array, and 54.0 DCI units for the 16-element array. For a 15-MHz signal at an elevation of 0.0° in the boresight direction these DCI units correspond to 0.91° and 4.96° of azimuth respectively. The main lobe of the 16-element array is thus 4.35 times wider than that of the 42-element array, clearly indicating that the long arm has the much better resolution capability.

5.2 Array Resolution

In order to determine the point at which two sources begin to be resolved, the DOPFUR program was modified to yield solutions for one source at a fixed position and a second source at a family of positions. A 2048-point FFT was used. The fixed source was assumed to be located in the approximate direction of the Texas transmitter, at a cone angle of 89.6° or at a direction cosine index (DCI) of 1020.0 with respect to the long arm. Calculations were carried out in which the second source was located at DCI = 993, 994,....1052, 1053. The DCI is used here since it is the same as the frequency bin index (k) in equation (1) which is dependent on the size of the FFT array and not the frequency. The DCI is converted to cone angle by equation (8). For a frequency of 15.0 MHz, the second-source DCI values correspond to cone angles from 85 ° to 92 ° with respect to the long arm.Calculations were carried out in which the power of the second source was 0.0 dB, -3.0 dB, -6.0 dB and -10.0 dB relative to that of the fixed source. The phase at the centre of the array arm was used to represent the phase of the source. The phase of the fixed source was arbitrarily set at 0.0° while the second source was given phases of 0.0°,

30.0°, ..., 360.0°. This second-source phase is thus also the difference in the phases of the two sources and is referred to as such.

The result of combining two sources can be visualized by using the curve in Figure 4 for the stronger source, displacing it for the second source both in position and magnitude and assigning it a different phase. The complex components at each DCI position are determined for each curve and the combined distribution curve calculated. At the different DCI positions there will be either constructive or destructive interference. The combined distribution will, in most cases, have its strongest peak at a particular DCI position corresponding to the main lobe of the strongest peak. At another DCI, there will be a second peak representing the main lobe of the second source, or an inflection indicating the presence of a second unresolvable peak. The positions of the peaks or the peak and the inflection will depend greatly on the phase difference between the two sources and the difference in the magnitudes of their main lobes.

The theoretical results indicated that as the angular separation of the two real sources was increased from zero, a point was reached where the unresolved determined sources became resolved. The separation of the real sources at this point for the 42-element array is plotted in Figure 11 as a function of the difference in phases of the two sources. The results for β ° are identical to that for (360 -β), where β is 0°, 30°,.....,360°. The separation in cone angle, for a frequency of 15 MHz, is indicated by the lowest of the horizontal scales; the scales above it indicate the positions of the sources in direction cosine index (DCI) and cone angle. The curve for -10 dB is dashed to indicate its uncertainty.

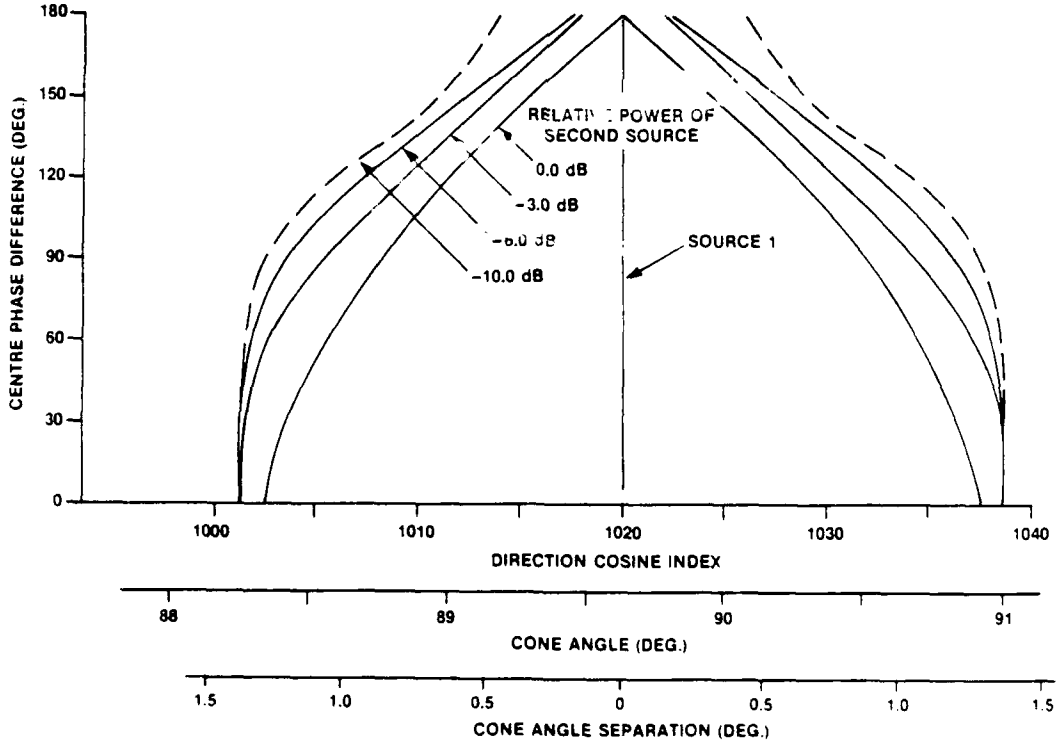

Figure 11. Minimum angular separation (lowest horizontal scale) required for resolution of two sources, as a function of the phase difference between the sources for various differences in source powers. First source is at DCI=1020, second source at contour. Frequency is 15 MHz.

Two important points are revealed by this plot. (1) With decreasing magnitude of the weaker source there is an increase in the width of the region where the two sources cannot be resolved. (2) As the phase difference between the sources increases from 0° to 180° (or decreases from 360° to 180°) the width of the unresolved region decreases, regardless of the magnitudes of the two sources. For signals with identical magnitudes and a 180° phase difference, the two signals remain separated up to the point of coincident locations, at which point the signals cancel and only noise remains.

5.3 Variation in Position of Unresolved Peak

The location of the unresolved single peak as a function of the difference in phases for two sources having the same magnitude is presented in Figure 12. The outer curves are the same as those in Figure 11, but here they approximately represent the second-source position where the two sources begin to be unresolved. The vertical dashed lines indicate the positions of the first and second sources, and are so labelled. The arrows start at these sources and both terminate at the line of the single combined peak. As can be seen, when the magnitudes of the two sources are identical, the unresolved peak appears midway between the two sources, and this location is independent of the difference in the phase of the two sources.

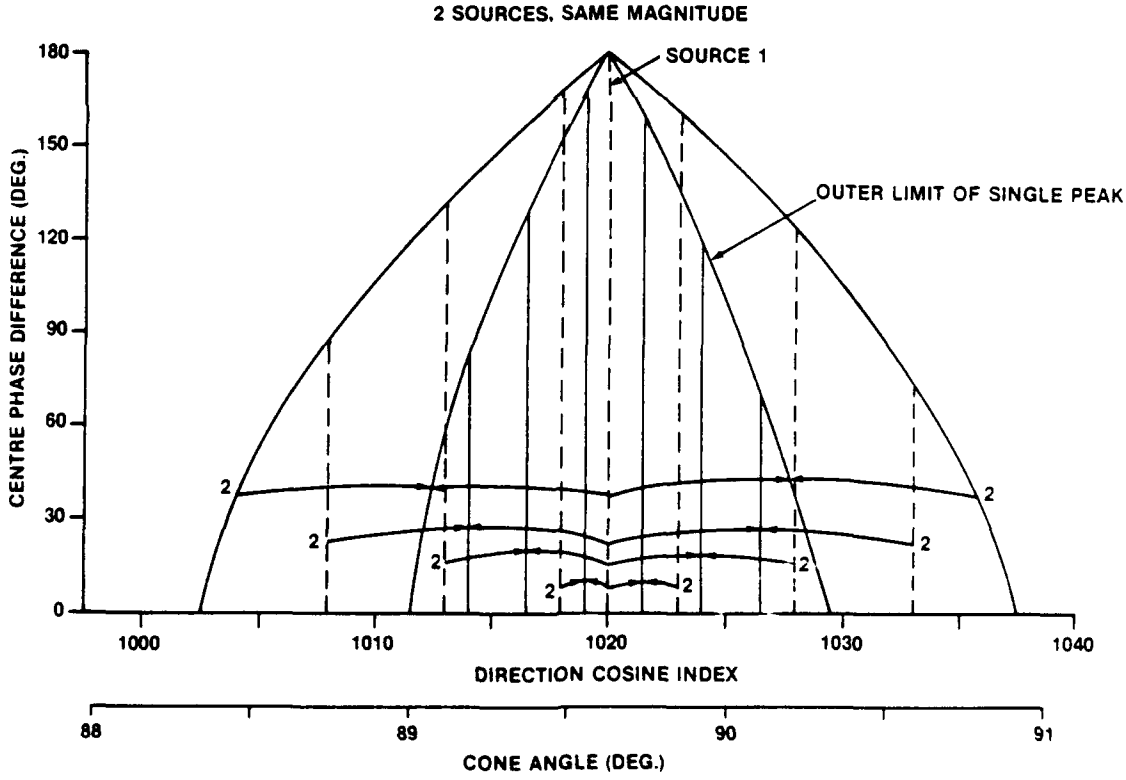

Figure 12. Location of unresolved single peak (where arrowheads meet) for first source at DCI = 1020 and second source at end of other arrow.

Figures 13 and 14 are similar to Figure 12 but the second source is weaker than the first source. As can be seen, for a weaker second source the unresolved peak is positioned between the two sources for phase differences less than 90°, but this position shifts to the reverse side of the stronger peak for larger phase differences. As the magnitude of the second source decreases, -3 dB in Figure 13 and -10 dB in Figure 14, the position of the unresolved peak quickly approaches that of the stronger source. In this range of magnitudes for the second source the position of the unresolved peak does not proportionately follow the position of the weaker source but behaves in an irregular manner. In Figures 13 and 14 the single peak for the second source at DCI = 1003 corresponds to the position of the first side lobe of the weaker source and the main lobe of the stronger source, while the single peak for the second source at 1013 corresponds to the position of the main lobe for both sources.

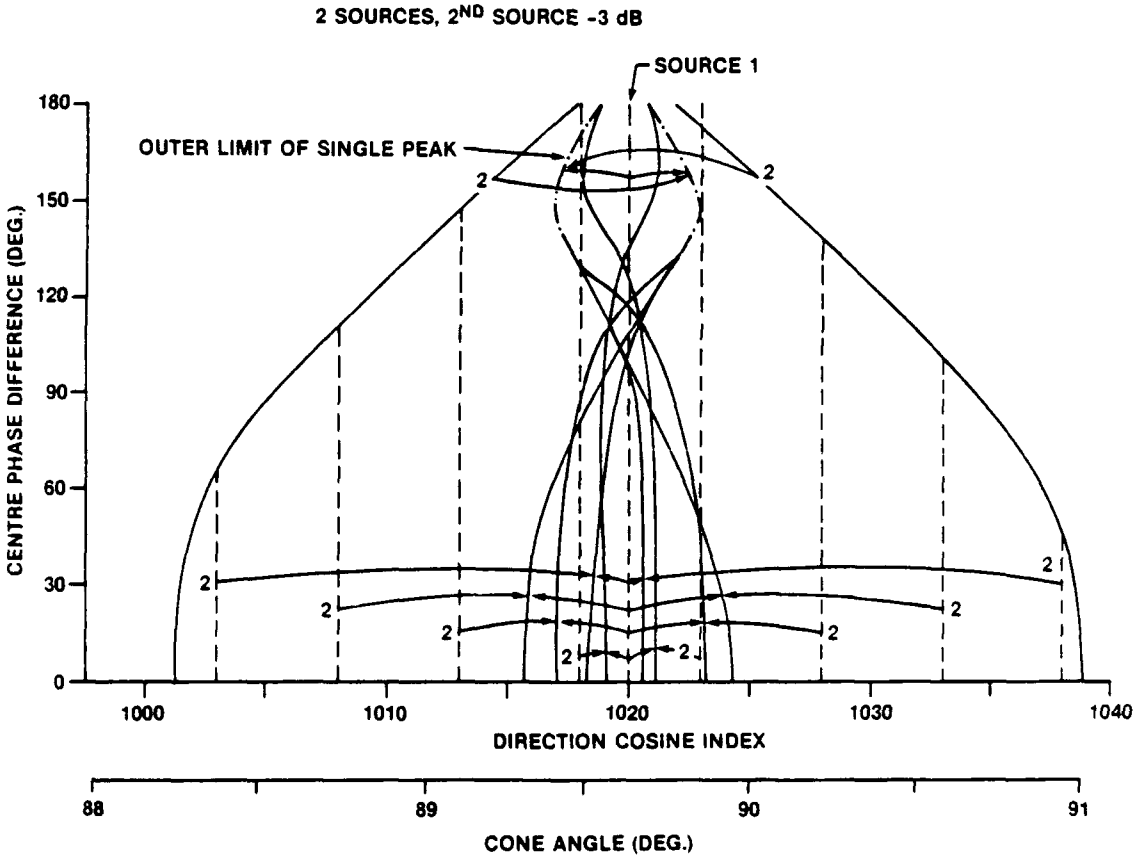

Figure 13. Location of unresolved single peak (where arrowheads meet) for first source at DCI=1020 and second source at end of other arrow.

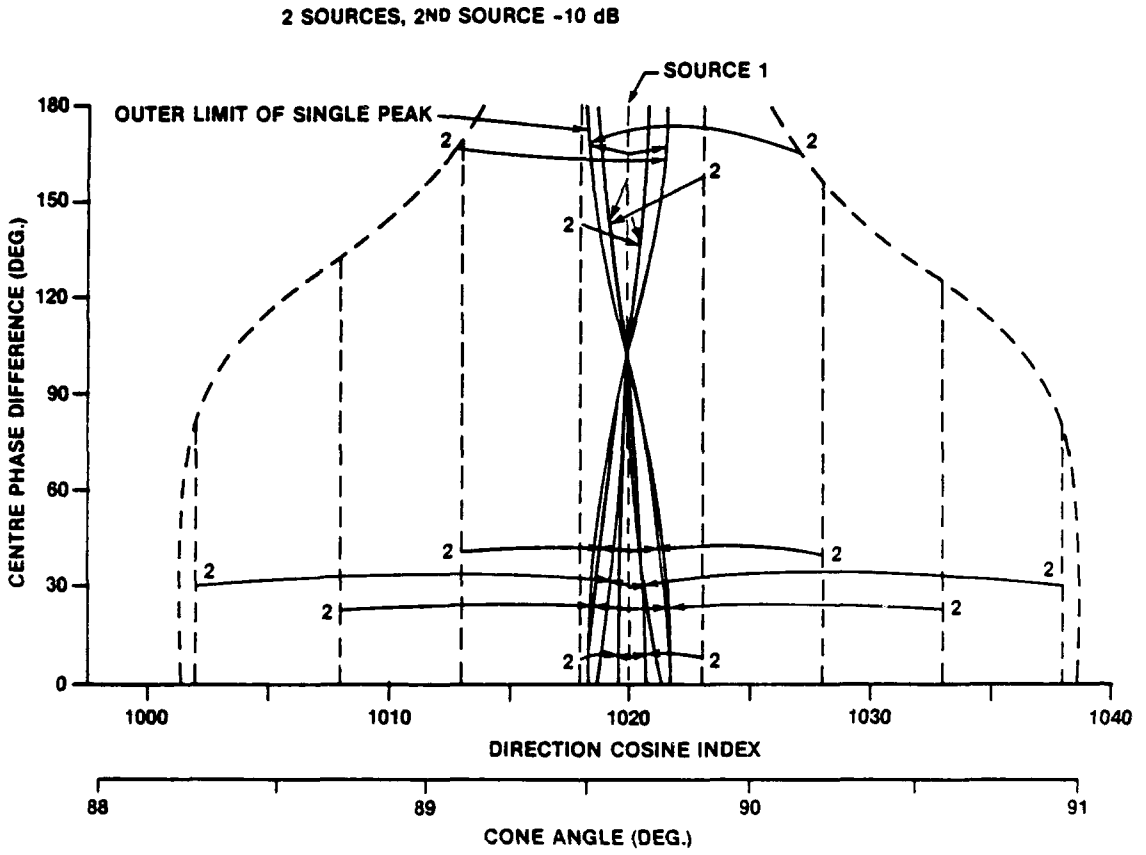

Figure 14. Location of unresolved single peak (where arrowheads meet) for first source at DCI=1020 and second source at end of other arrow.

5.4 Effect of Noise

The effect of different levels of background noise was investigated. An increase in the background noise (a decrease in the signal-to-noise ratio) introduces a "jitter" in both the phase and magnitude of the received signal which appears in the post-FFT result. With increasing noise it becomes increasingly difficult to identify the exact cone angle positions of either the resolved or unresolved peaks.

5.5 Possible Accurate Bearings During Multipath

The results in Figures 13 and 14 also indicate that there is a narrow range of centre phase differences near 100° (or 260°) where the location of the unresolved peak is very near that of the stronger source regardless of the magnitude and position of the weaker source. What happens under these conditions is that the vector sum of signals in the vicinity of the main lobe of the strongest signal produces a narrower main lobe than would be produced for a phase difference closer to 0.0°. This result suggests that during multiple-source and/or multipath conditions it may be occasionally possible to obtain a correct bearing. The

phase difference between the two strongest sources would have to vary with time and the phase difference would have to pass through 100 or 260 °. If a number of bearings were determined near that time, their standard deviation would be small. This result could be applied to situations where an accurate direction-of-arrival estimate is required and multipath is present. Work with real-world signals is needed in order demonstrate this finding and further develop the technique.

5.6 Sky Positions of Peaks From Two Array Arms

Once a peak on one array arm is matched to a peak on the other array arm, the elevation and bearing or sky position of the source can be determined. A study of the change in this sky position when one source is fixed and a second is variable can reveal much about the resolution limit of the FFT. A special version of DOPFUR program was used to investigate this matter. Signals present at each element of the SARA array were generated in a simulation program using known bearing, elevation, amplitude and phase values for the two sources. Noise was not included. For this study both sources were set at an elevation of 10.0°. The first source was set at a bearing of N 236.42 E, the bearing of the Texas transmitter, and calculations were carried out for the second signal at bearings N 230.42 E to N 241.17 E in 0.25 degree steps. A frequency of 14.55 MHz was used.

Figure 15 illustrates the results for the 42-by-16-element array for the case where the phases and magnitudes of the two sources are identical. At this stage points have not yet been removed on the basis of (1) the difference in the phase of the peaks on the two arms exceeding the 45-degree limit or (2) the amplitude of the peak on one arm exceeding that on the other arm by more than 10 dB. In this figure, the first source is located at N 236.42 E at the position of the arrow and the second, in sequence, at the numbered points on the 10.0-degree elevation line. The other numbered points indicate the corresponding determined or apparent source positions. For the second source located at positions 1 to 19 and 30 to 44 the analysis indicates that the determined second apparent source would appear along a curve whose locus runs between 11 degrees elevation at N 230 E and 8 degrees elevation at N 240 E, which is close to a cone angle of 10 degrees to the SW to NE arm. The apparent first source would appear along the N 236 E bearing between elevations 9 degrees and 12 degrees which is close to a cone angle of 84 degrees to the NW-to-SE arm. For positions 20 to 29 only a single apparent source appears. For positions 3 to 9 and 40 to 44 a clearly erroneous third apparent source appears near an elevation of 10.2 degrees at bearings near N 234 E and N 239 E respectively.

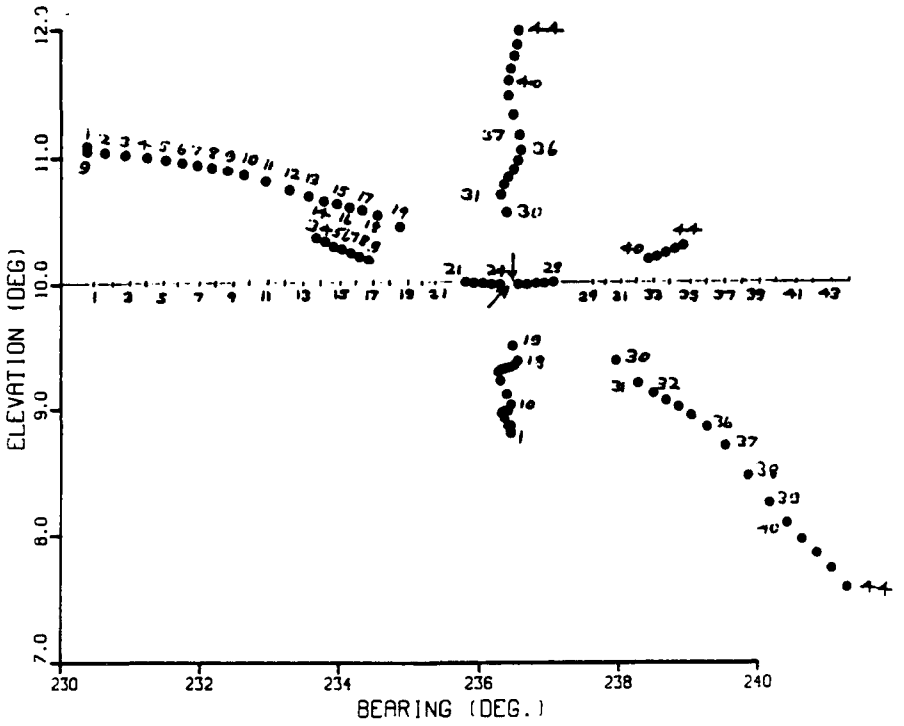

Figure 15. Display of apparent locations of two sources for various actual positions of sources. Sources have equal magnitudes and both are located at 10 degrees elevation. The actual position of the first source is indicated by the arrows, and the numbers along the 10 degree elevation line indicate the positions of the second source. Numbered dots indicate determined apparent positions of sources. Frequency is 14.55 MHz.

Figure 16 is the same as Figure 15, but now only those cases with matching centre phases and matching amplitudes are plotted. It is now clear that there are missing positions for the apparent first and second sources. The sky positions which are missing for the first source (vertical line of points) correspond to the positions of the nulls of the radiation pattern of the second source, while those which are missing for the second source correspond to the positions of the nulls of the radiation pattern of the first source. Signals located at such positions were normally too weak to be reliably identified as possible sources, and criteria inserted in the DOPFUR program prevent such weak signals from being identified as sources.

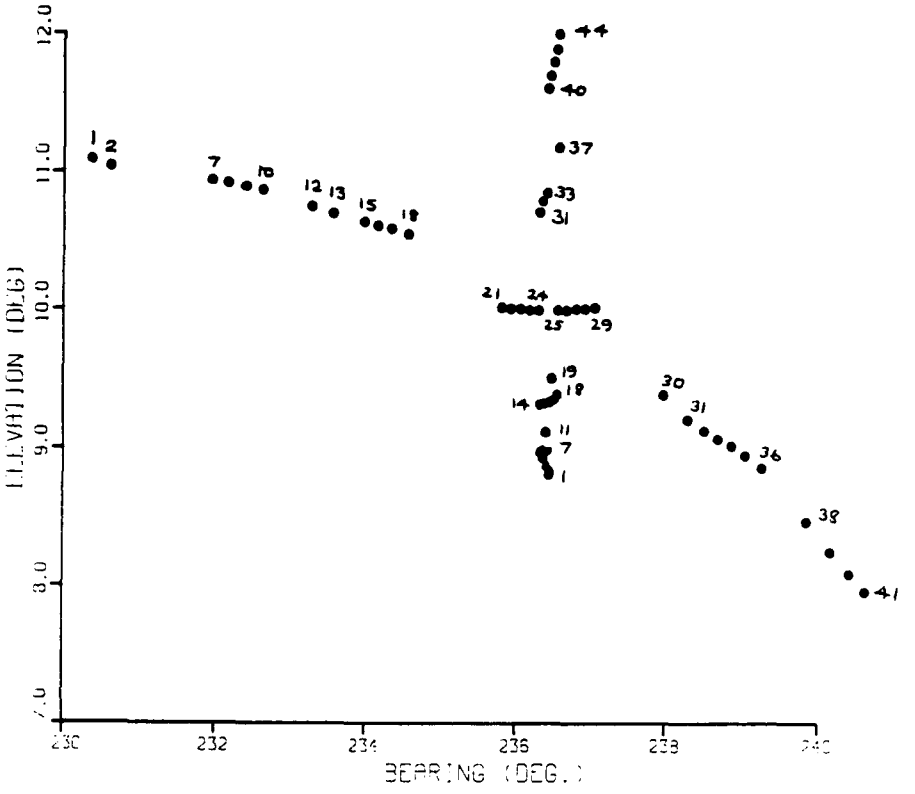

Figure 16. Sources plotted in Figure 15 which were acceptable.

Upon examination of Figures 15 and 16 it is clear that sources can go undetected if located at certain positions in the sky and that the source positions determined can be several degrees off the true sky position.

Plots (not shown here) were also prepared for cases where the two peaks had equal magnitudes but had differences in the centre phases of 40.0° and 170.0°. For the former the results were similar to that in Figures 15 and 16 whereas for the latter the phases of the two sources were nearly reversed and for the source positions used in Figure 15, apparent source positions could be found in only a few cases.

The main conclusion drawn from these figures is that there are weaknesses in the FFT technique for identifying sources. When two equal-amplitude sources are present there will be certain rare locations of the two sources, e.g. position 3 for the second source in Figure 15 at a bearing near N 231 E for which, as indicated in Figure 16 no apparent source could be confidently identified. As well, there would be selected positions of the second source, e.g. 1, 8, 9, 17, 18, 31 to 33, 40 and 41 for which both sources could be confidently identified. At such locations the side lobe of one of the sources will usually coincide with the main lobe of the other source. As the difference in the phase of the two sources increases the signals of the two sources will interfere more seriously with each other and fewer positions of the determined sources will be found.

confidently identified. At such locations the side lobe of one of the sources will usually coincide with the main lobe of the other source. As the difference in the phase of the two sources increases the signals of the two sources will interfere more seriously with each other and fewer positions of the determined sources will be found.

For a second signal which is weaker, fewer second-source positions will be identifiable, and these will all be at one of the side lobes of the stronger source. Clearly, the positions of sources as obtained from the FFT analysis are significantly biased by the side lobe structures of the other sources that are present.

6. Experimental Results of DOPFUR Analysis Program Using PI Technique

6.1 Experimental Technique

The experimental setup and the measurements reported below are described in Montbriand (1981). Both a swept frequency continuous wave (SFCW) or chirp signal and a fixed frequency or beacon signal were transmitted from San Antonio, Texas (29.45 °N, 98.62° W) and received at Ottawa (45.23° N 75.85 °W) over the period Nov. 25 - 27, 1977. The signals were received by a 62-element 1943-m by 236-m crossed array with the short arm oriented at a bearing of N 49.7 E. Further details are given in Montbriand (1981) and Rice and Winacott (1977). The chirp signals were processed by Montbriand (1981) and the results presented in that report.

6.2 DOPFUR Results

The beacon results were preprocessed into 256 Doppler frequencies. The DOPFUR program was used to examine this data. Normally the frequency distribution was very narrow and the expected signal occupied only a few of the Doppler frequency bins. To identify those bins, for each Doppler frequency the average of the signals at the antennas was calculated. From the amplitude distribution the largest isolated peaks were identified. Only those peaks within an arbitrary power range of that of the largest peak (specifically, within 10 dB) were believed to contain the expected signal and were processed to identify sources. The Doppler frequencies of the peaks were usually less than one Hz, but cases of several Hz were sometimes identified, and these usually corresponded to strong interferers or signals which were side-scattered.

The experimental results over the period Nov. 25 - 27, 1977 were examined. Based upon the forward scatter ionograms and the chirp results it was found that the signal received contained multipath and multi-mode propagation components. Sources with amplitudes spanning 40 dB could be identified using the chirp signals which, as will be shown, is some 20 dB better than could be done with the beacon results. (The chirp signals permitted sources to be separated on the basis of propagation data; this was not possible for the beacon signal.) Over the time intervals examined, propagation via the F2 layer over both the low-angle and high-angle paths was present on 184 one-minute intervals. Propagation via the F2 layer over a single low-angle path in combination with multiple high-angle paths, such as occurs during travelling ionospheric disturbances, was present on 140 one-minute intervals. Propagation via two hops off the F2 layer in conjunction with any combination of one-hop propagation was present on 222 one-minute intervals. Propagation via the F2 layer, when the radio frequency was at the MUF of the layer, was present on 55 one-minute intervals.

The same beacon signals were processed using the DOPFUR analysis. This program normally examines Doppler signals down to 10 dB below the strongest signal, below which the signal contains too much multipath and too much noise to unambiguously

separate sources. For each Doppler signal examined, directional peaks down to 10 dB below the main directional lobe were processed to identify sources. Below that level sources could not be unambiguously identified. The maximum range of amplitudes was thus 20 dB, half the 40-dB range of the chirp analysis. As a consequence, most of the weaker signals Montbriand (1981) identified using the chirp analysis were not identifiable using the DOPFUR analysis.

The beacon results can be summarized as follows: (1) During normal propagation conditions, the Doppler frequency distribution was usually very narrow, exhibiting a single strong peak. Multipath and multimode propagation, when present, usually exhibited the same Doppler frequency as that of the dominant propagation mode. Such modes usually had intensities more than 10 dB below the strongest directional peak and hence were not identifiable by the DOPFUR analysis. (2) When multiple paths from the F2 layer via the high-angle path were present, clearly defined multiple traces of the same propagation mode were present on the ionogram. These multiple traces usually exhibited similar powers but had different Doppler frequencies and different sky positions (i.e. elevation and bearing). (3) When two-hop propagation via the F2 layer was present the trace was smeared over a long time delay. Peaks at more than one Doppler frequency were identified on 75% of the one-minute intervals, and a third of these were the result of two or more sources. (4) The case of the MUF is unique. At frequencies just below the MUF, the Doppler frequency distribution was found to be broad and many Doppler peaks could often be identified within 10 dB of the largest peak. The signals from some of these peaks were the result of several sources. (5) For radio frequencies just above the MUF the Doppler frequency distribution was largely that of noise plus interference and all sorts of frequencies and source locations were usually found.

In general, the direction-of-arrival of a signal which was propagating essentially in the great circle direction could be determined at all times when the radio frequency was below the MUF; in many cases such propagation could be determined at more than one Doppler frequency. In 20% of the cases the signal present at a particular Doppler frequency could be separated into two or more sources. The only time the expected source could not be identified was when the signal had vanished into the background noise due to the radio frequency being above the MUF. The sky positions obtained using the DOPFUR analysis on the beacon data were similar to those obtained by Montbriand (1981) for the chirp data; they were not identical as the two sets of data were recorded 20 seconds apart. The direction-of-arrival precision of the beacon results for the Doppler-frequency-separated data and the time-equivalent data are almost identical. This is discussed in the next section.

7. Experimental Results of TIMFUR Analysis Programs Using PI Technique

A study similar to that detailed in Section (4) was carried out on specially prepared time-equivalent data.

The time-equivalent data was prepared from the received beacon data. This data was converted to complex voltages by first-order phase and amplitude corrections, followed by corrections for phase and amplitude differences resulting from differences in cable lengths. This was the data processed by the TIMFUR analysis program.

Corrections not performed were the radio-frequency-dependent corrections. These included the obvious correction for the 4.0 Hz offset which had been used to shift the received signal away from 0.0 Hz. Another correction not made was that due to the Doppler shift of the received signal; instead, this was regarded as a parameter to be measured. One final correction was that for the time delay between the sequential sampling

The results for Nov. 25 (day 329), 1977 for 10:29:20 EST are presented in Figures 17 to 21. A restricting cone angle window was not used so that the possibility of detecting sources would be increased. The time history of the bearings and elevations are presented in Figures 22 and 23. The signal frequency was 14.45 MHz.

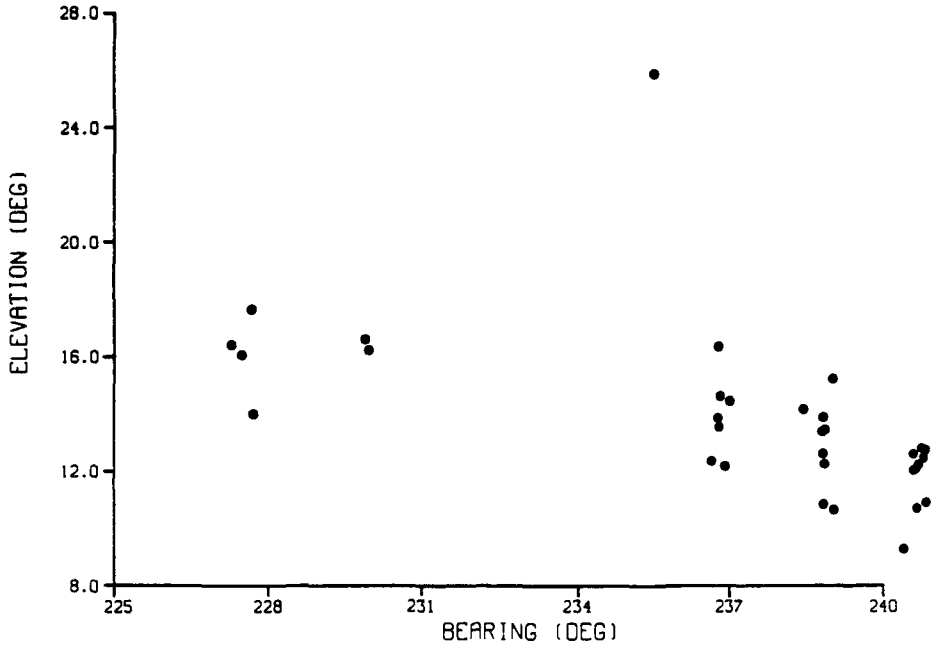

Figure 17. Best solution sky positions of sources on day 329 at 10:29:20 EST for scans 1 to 11. Frequency is 14.45 MHz.

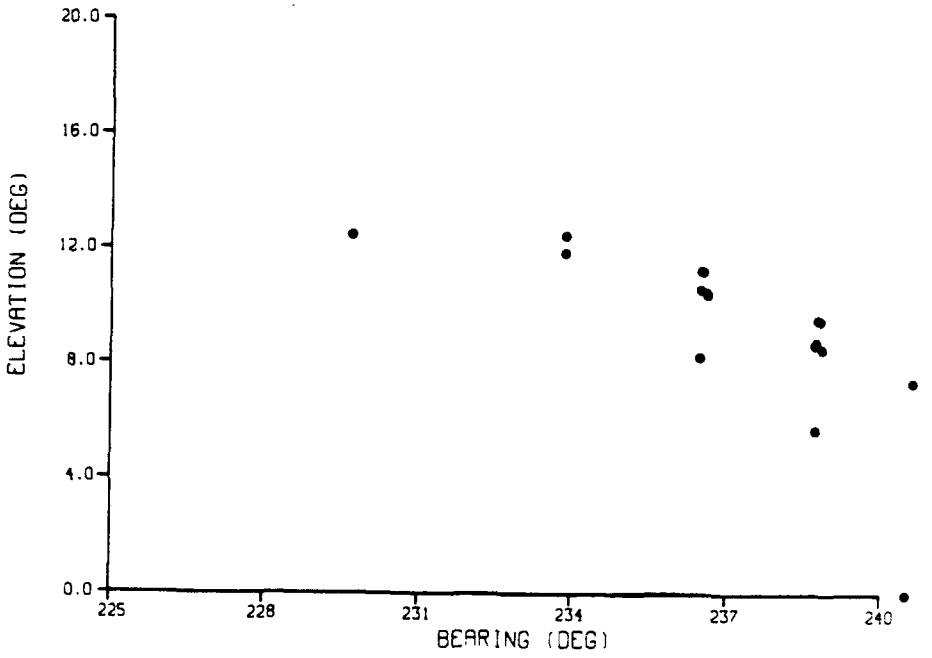

Figure 18. Best solution sky positions of sources on day 329 at 10:29:20 EST for scans 12 to 18.

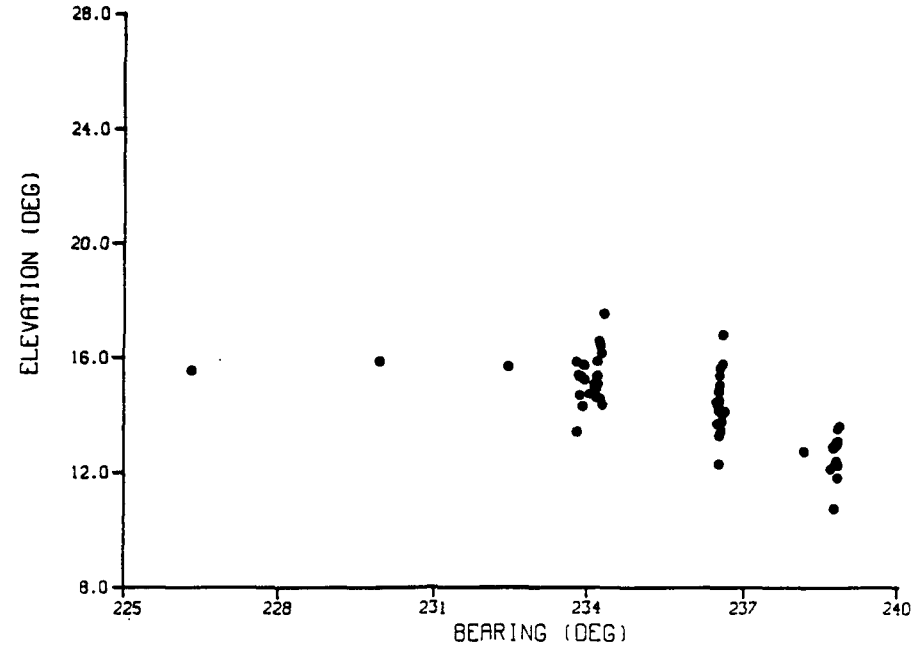

Figure 19. Best solution sky positions of sources on day 329 at 10:29:20 EST for scans 19 to 41.

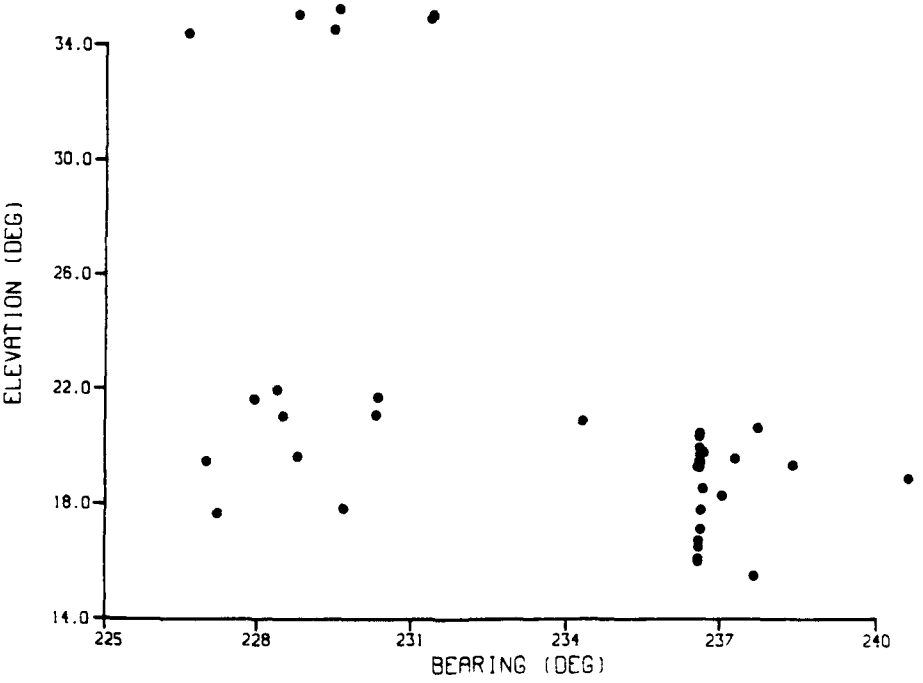

Figure 20. Best solution sky positions of sources on day 329 at 10:29:20 EST for scans 46 to 83.

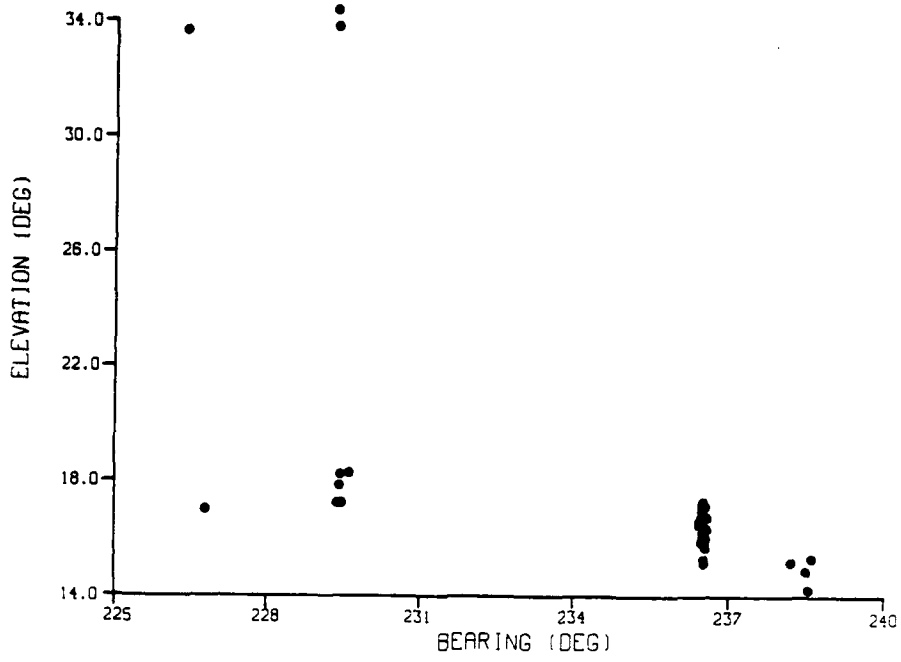

Figure 21. Best solution sky positions of sources on day 329 at 10:29:20 EST for scans 84 to 125.

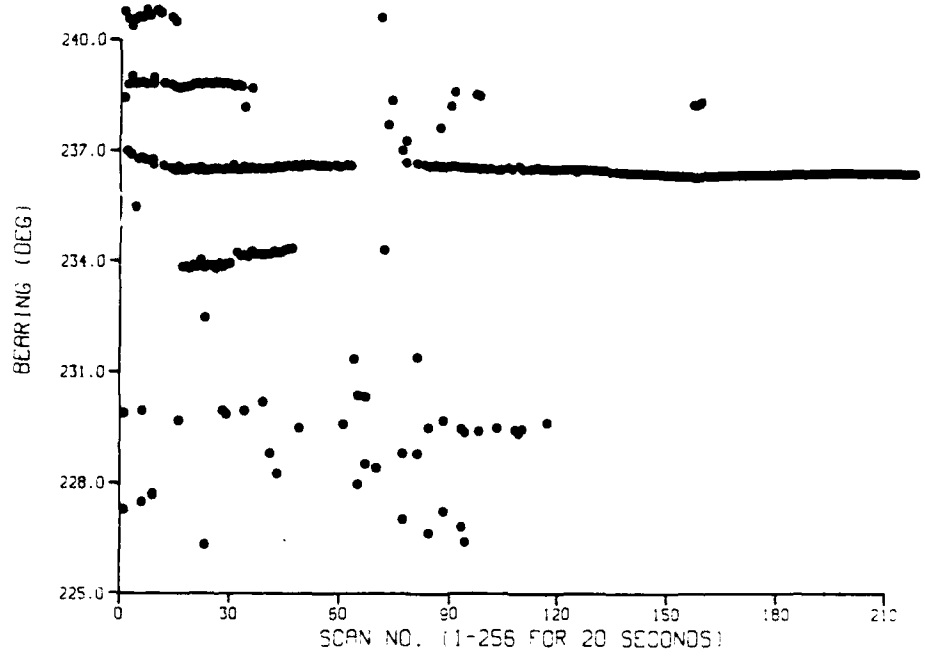

Figure 22. Bearings of all sources from best solutions on day 329 at 10:29:20 EST for scans 1 to 218. Frequency is 14.45 MHz.

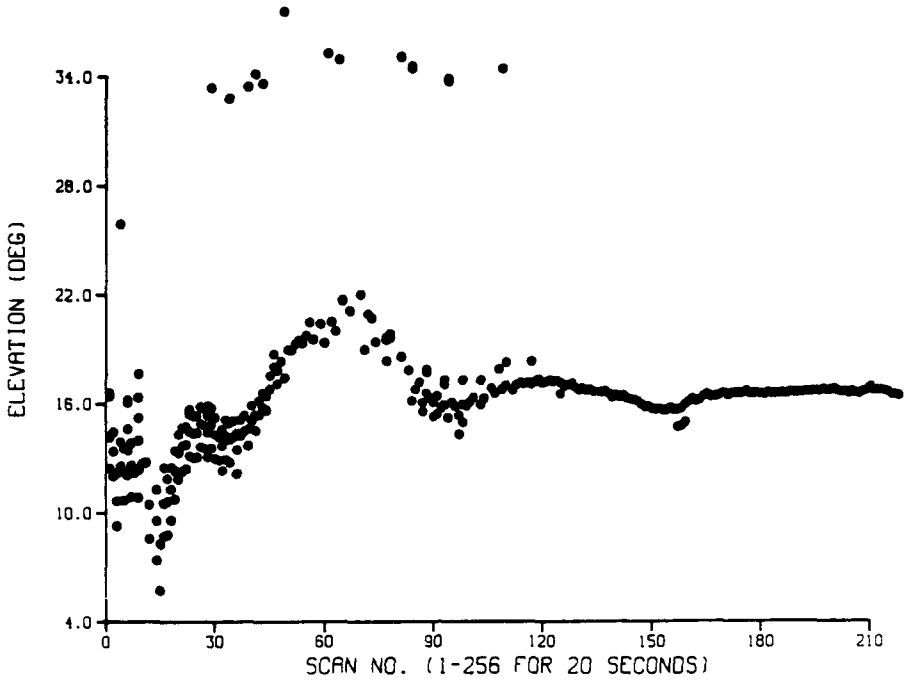

Figure 23. Elevations of all sources from best solutions on day 329 at 10:29:20 EST for scans 1 to 218. Frequency is 14.45 MHz.

The results in Figures 17 and 22 for scans 1 to 11 (of the 218 usable scans in the one-minute interval) indicate possible sources at bearings of N 236.8 E, N 238.7 E, and N 240.5 E. The results in Figures 19 and 22 for scans 19 to 41 indicate possible sources at 234.2, 236.8 and 238.8 degrees. The results in Figures 21 and 22 for scans 84 to 125 indicate possible sources at 229.5 and 236.5 degrees. For scans 125 to 215 there was a single source near 236.5 degrees.

The multiple bearings listed above were suspiciously regular in their spacing. A careful study was carried out to determine if the sources were real, and if so, why their bearings were so distributed. The study revealed that the strongest source was located near N 236.8 E. It also revealed that for scans 1 to 47 (c.f. Figures 22 and 23) severe multipath was present. There were 1 to 20 possible solutions for each scan, and of the first 47 scans, 12 had 3 or less possible solutions. The second and third sources on scans 1 to 11 have amplitudes which are about -3 dB and -5 dB of the first source, well above the -14.5 dB side lobes on both sides of the main lobe. For each source the centre phase difference was also small, indicating that the separate sources were real. It was concluded that the seemingly regular spacing between the three sources was a result of the bias that the side lobes would introduce for the position of weaker secondary and tertiary sources, the effect discussed earlier and illustrated in Figures 15 and 16. In the present case the strongest source is located near N 239 E for the first few scans and near N 237 E for the remaining scans. The other positions appear to be side-lobe positions of the strongest source and are the biased locations at which the second and third sources would be identified. Precise locations for all three sources may require superresolution techniques for their identification.

7.1 Use of Doppler Frequency for Source Identification

The TIMFUR results contain another feature which can be used to establish the uniqueness of different sources when multiple sources are present. Each source has its own Doppler frequency and this frequency can be estimated from a time history of its mid-array phase. As an illustration, if the scan rate was 12.8 Hz (as was our case) and if the time history indicates a source has a phase rotation of -120° between scans, then the total frequency difference is (-120./ 360.) x 12.8 Hz = -4.27 Hz. Removing the 4.0 Hz offset leaves a Doppler shift of -.27 Hz for the source. Other sources can be similarly identified. This suggests that a useful comparison of these source-Doppler results could be made with the sources obtained from the DOPFUR analysis. Such a comparison was not always possible to achieve because the TIMFUR results often had a time varying Doppler frequency and existed for only a short time whereas the DOPFUR results were on average over 218 scans. Short-lived sources were not identifiable in the DOPFUR results; they would have appeared as sources too weak to be detected. As a consequence, only a rough comparison of the results could be made. Only those sources which were intense and persisted for a long time could be matched to the TIMFUR sources. Multiple sources in the DOPFUR results corresponded to fairly stable sources in the TIMFUR results.

8. The MUSIC Algorithm

The MUltiple SIgnal Classification (MUSIC) algorithm of Schmidt (1981) has become one of the latest signal processing tools for separating signals which are closely spaced in bearing or elevation or for identifying a weak signal in the presence of a strong one. It was these characteristics which motivated a cooperative project between the Communications Research Centre (CRC) and the Naval Oceans Systems Center (NOSC). The objective of this project was to use data obtained by the SARA facility during a propagation experiment over a Texas-to-Ottawa path in 1977 to study the direction-of-arrival limitations of the MUSIC algorithm, the wavefront testing technique and the FFT algorithm technique. The studies were to be carried out on identical data. NOSC was sent specific data so as to examine the potential of the MUSIC algorithm. In return, CRC was to receive copies of the MUSIC algorithm software. At CRC the wavefront testing technique was studied by Winacott (1986) and the FFT algorithm technique by the author. the results of which are included in this note. The MUSIC software somehow did not arrive, and faced with a slim hope that it would arrive before termination of this project* the author investigated the possibility of preparing his own. Thanks to the cooperation of Dr. Eric Hung (1986), the author was able to obtain a general layout of the computations of the MUSIC algorithm (see Appendix A). Based on this layout the author was able to successfully prepare a computer program called TMUSIC for processing time equivalent data into directions-of-arrival estimates. The computer program calculates the directional distribution of the received signal at selected elevations. The locations of the various peaks and their amplitudes for these elevations are used to determine the sky positions of the various sources. A logical extension of this software would be to use an iterative procedure to identify the precise elevation and bearing of each source present in the received signal.

* A final report, "Signal Subspace Processing of Actual Radio and Acoustic Data" by G.E. Martin, 213pp, Martin Analysis Software Technology, Inc., San Diego, Calf., Feb. 1988, arrived Dec. 12, 1988

9. Results of the MUSIC Program

9.1 Results Based on Simulated Data

A simulated signal identical to that which would be picked up by the SARA array was calculated using a program called DOPSIM. Up to five separate signals could be combined and white Gaussian noise could be added to it to provide a pre-specified signal-to-noise ratio. Such signals were generated for all 256 Doppler frequency bins. The parameters of each signal were as listed in Table IV and are the source's bearing, elevation, signal amplitude, and phase that the signal would have at the centre of the crossed array. For the test, the noise was set at 40 dB below the strongest signal. Signals from the three sources listed below were used with tests carried out on one, two and three sources.

Table IV

Description of Sources Used in Tests

Source	Bearing (Deg.)	Elevation (Deg.)	Amplitude (μV)	Centre Phase (Deg.)
1	235.00	15.00	10.0	45.0
2	225.00	15.00	10.0	100.0
3	245.00	15.00	10.0	155.0

A frequency of 15.0 MHz was used. The simulated data was first analyzed using the DOPFUR program and the results are presented below.

Table V

DOPFUR Results of Tests

Sources	Bearing (Deg.)	Elevation (Deg.)	2 Arm Amp. Diff. (dB)	Centre Phase Diff. (Deg.)
1	234.99	14.99	0.2	0.2
1, 2	224.97	15.07	5.1	-25.8
	235.00	14.90	5.1	-25.8
1, 2, 3	224.93	16.48	6.0	3.2
	235.05	16.32	6.2	-49.2
	244.64	8.54	6.1	54.8

The simulated data was then processed using the TMUSIC program. Using forward-sequenced data, the result in each case was essentially the same as obtained by the DOPFUR analysis. This is because the MUSIC algorithm requires a measurable degree of uncertainty in each of the signals for the algorithm to function properly. Adding varying degrees of noise was tried but these did not help, probably because the signal was still too pure. Introducing amplitude and phase jitter into the simulated signal would likely have produced satisfactory results. Before this was tried, however, it was found that a superior solution could be obtained using forward- and reverse-sequenced data, as described below.

A procedure which is commonly used if the samples are evenly spaced is to combine the covariance matrices of forward-sequenced data and conjugate reverse-sequenced data. The samples used in our experiment were not evenly spaced but were so spaced that the conjugate reverse-sequenced data matched the signal and phase pattern of the forward-sequenced data, permitting their use in such a combined covariance matrix. The fact that the reverse-sequenced data did not produce a perfect match to the noise from the forward-sequenced data was advantageous in that it allowed the MUSIC algorithm to benefit from the additional, seemingly independent reverse-sequenced data. In cases where the MUSIC algorithm performs satisfactorily using the normal forward-sequenced data, inclusion of the reverse-sequenced data reduces the incoherent noise and amplifies the coherent signal. In this work, very good results were obtained from the combined covariance matrix. Using such a matrix, the MUSIC algorithm produces a signal variation with direction cosine which is an improved version of that produced using the FFT algorithm. For a single source the locations of the various lobes and nulls are essentially identical to those obtained using the FFT algorithm, but the magnitudes of the grating and side lobes are depressed with respect to the main lobe. With two sources, the spatial resolution is much better than that produced using an FFT. For certain source locations the MUSIC algorithm can determine the applicable sky position more accurately than the FFT. In some cases where the FFT could only identify a broad source, two sources could be identified by the MUSIC algorithm.

In Table VI are presented results for 1, 2, and 3 sources using the MUSIC algorithm, results which can be compared to those in Table V.

Table VI

TMUSIC Results of Tests

Sources	Bearing (Deg.)	Elevation (Deg.)	Amplitude (dB)	Amp. Largest Side Lobe (dB)
1	234,74	15.01	0.0	-36.2
1,2	224.74	15.01	0.0	-36.2
	234.75	15.02	-0.3	
1,2,3	235.54	13.13	0.0	-12.4
	244.79	13.80	-1.06	
	224.59	16.54	-2.49	

The results for a single source indicate that the TMUSIC program has introduced a small systematic bearing error of 0.25 degrees. A careful review of the program and the nature of the results expected clearly indicated that the program functioned properly. However time was not available to isolate the source of the 0.25-degree error. After removing this error, the TMUSIC sky positions and strengths are almost perfectly matched in amplitude and position to the actual positions for the two sources. The TMUSIC program yields better sky positions than can be obtained using the DOPFUR analysis. This is even more evident for the three sources whose mean angular error (vector sum of horizontal error, i.e. bearing error times *cos*(elevation), and vertical error) is 3.08 degrees for the DOPFUR results and 1.58 degrees for the uncorrected TMUSIC results. The amplitudes on the two arms are poorly matched in the DOPFUR results and very closely matched in the TMUSIC results. Thus the MUSIC algorithm is a substantial improvement over the FFT algorithm. The work of Martin (1988) confirms these findings.

What is also clearly evident is that using the MUSIC algorithm to process data containing signals from three sources does not necessarily yield a near perfect solution; there is still a substantial error in the estimated sky position of each source. Grooming of the data as indicated by Martin (1988) will reduce the error, but a measurable error still remains. Termination of this project made it impossible to look into this and related problems.

9.2 Experimental Results Using the MUSIC Algorithm

The TMUSIC and DOPFUR analysis programs were used to process some of the time equivalent data of Nov. 25 (day 329), 1977. Details of the minute interval at 10:32:20 EST are discussed below. The frequency was 14.45 MHz. The DOPFUR analysis for scans 1 to 10 of the 256 scans indicated that only one source was present and that it was located at a bearing of N 235.14 ±.09 E, at an elevation of 18.15 ±.27°. The TMUSIC results, when processed for just the forward sequencing of the data suggests the presence of more than one source, but yields only one sky position which was at a bearing of N 234.95 E at an elevation of 18.22°. When both the forward and backward sequencing of the data is used, the possibility of separating two closely spaced sources increased. As indicated below, for the data examined, two sources were identifiable.

Solution of the n x n covariance matrix yields n eigenvalues and n corresponding eigenvectors. The largest eigenvalues belong to what is referred to as "signal space" and the remainder to "noise space". There appears to be no clear separation between the signal and noise spaces although the smallest eigenvalue of the signal space is usually taken to be a factor between 10^3 and 10^4 less than the largest eigenvalue. The treatment used herein uses eigenvectors of the signal space, whereas Martin (1988) used eigenvectors of the noise space. The approaches are different but they both appear to yield the same result. The number of eigenvalues of the signal space to use is usually taken to be a few more than the number of expected sources. If too few or too many eigenvalues are used in the solution, the result is inferior.

For the test conducted the number of eigenvalues (and their eigenvectors) corresponding to the signal space was found to be more than 4 and less than 20. Many of the eigenvalues clustered near a certain value and it was found best to either accept or reject them as a group. For minute 10:32 almost identical sky positions were obtained using 7 and 11 eigenvectors. This problem is studied by Martin (1988). A strong source was found at a bearing of N 234.9 E at an elevation of 18.7° and a second source, with a magnitude 5.9 dB weaker at a bearing of N 239.1 E and elevation of 17.5 °. The strongest side lobe was 14.3 dB weaker than the strongest signal. According to the chirp results and the corresponding ionograms, both of these sources were the low-angle path of the two-hop propagation mode of the F2 layer.

In order to obtain a more complete illustration of the potential of the MUSIC algorithm for identifying all sources, the TMUSIC program was used to determine the azimuthal variation of intensity for the minute interval at 10:30:20 EST for all elevation angles from 0 to 90° in 1° steps. For each elevation the locations of all of the peaks were determined. All peaks within 16 dB of the intensity of the largest peak are plotted in Figure 24. This plot has the zenith at the centre, the horizon as the outer circle, elevation circles in 5-degree steps and bearing lines in 5-degree steps. On this figure the thick lines correspond to amplitudes 0 to -11 dB, the thin lines -11 to -15 dB and the dots to -15 to -16.2 dB. Two sources were identified, the stronger at a bearing of N 235.6 E at an elevation of 19.6° and the weaker with a bearing of N 227.5 E at an elevation of 19.2°. All

other maxima are grating lobes, side lobes and aliased main lobes. Figure 25 extends the results plotted in Figure 24 to include all peaks above -17.8 dB. There is a pattern in the locations of the peaks; the sources are located on a cone angle (CA1) running from the lower left to the upper right and the peaks along CA1 have predictable relative locations and magnitudes. Each of the peaks along CA1 correspond to the strongest peak in the amplitude distribution along the cone angle of the other arm (CA2) running from the upper left to the lower right. Peaks along CA2 also have predictable relative locations and magnitudes. In Figures 24 and 25 two sources are present and their combined signal, in places, conceals this pattern. As can be determined from Figure 24, almost all of the peaks are below -11 dB.

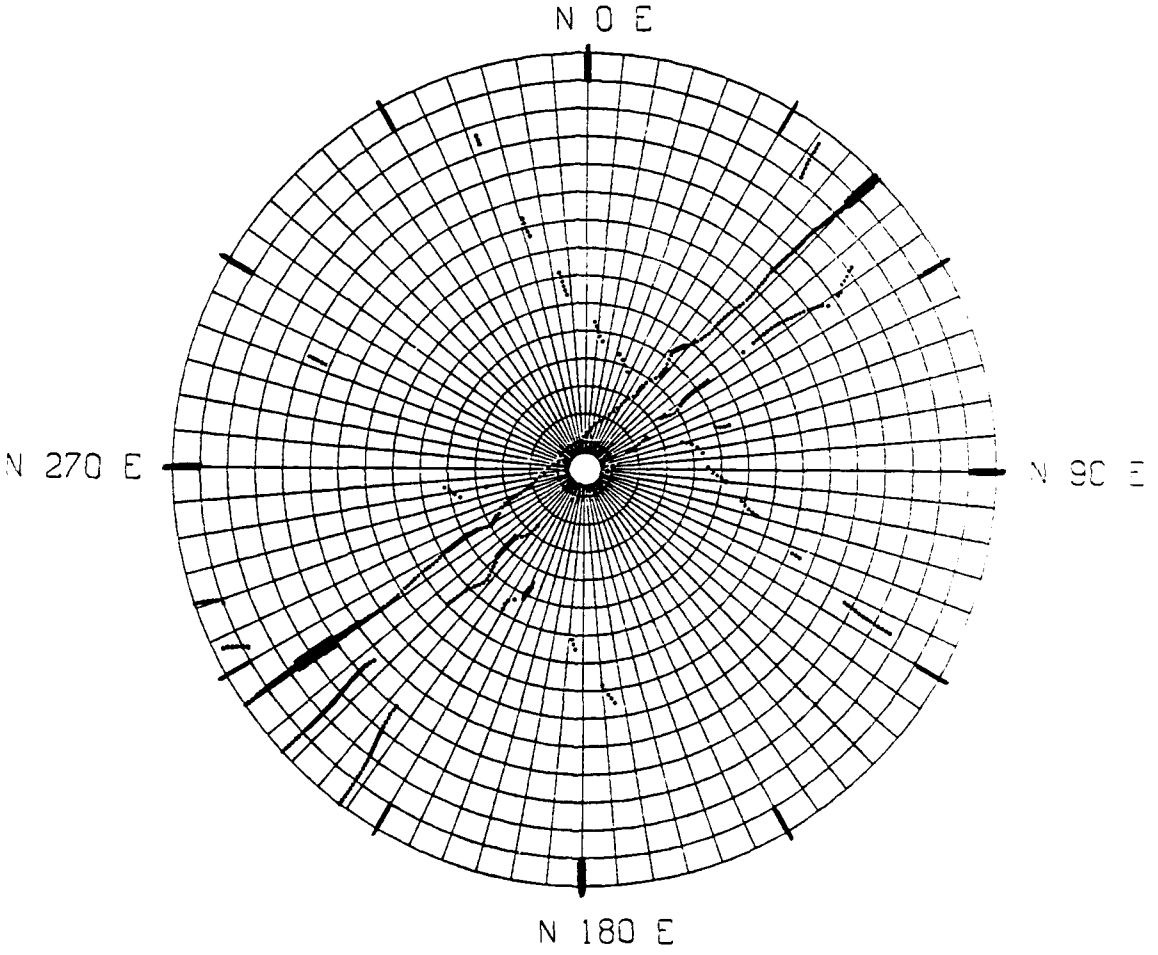

Figure 24. Sky plot of all peaks of TMUSIC for Nov. 25, 1977 at 10:30:20 scans 119-130. Legend: Thick line 0 to -11.0 dB, thin line -11.0 to -15.0 dB, dots -15.0 to -16.2 dB. Frequency is 14.45 MHz.

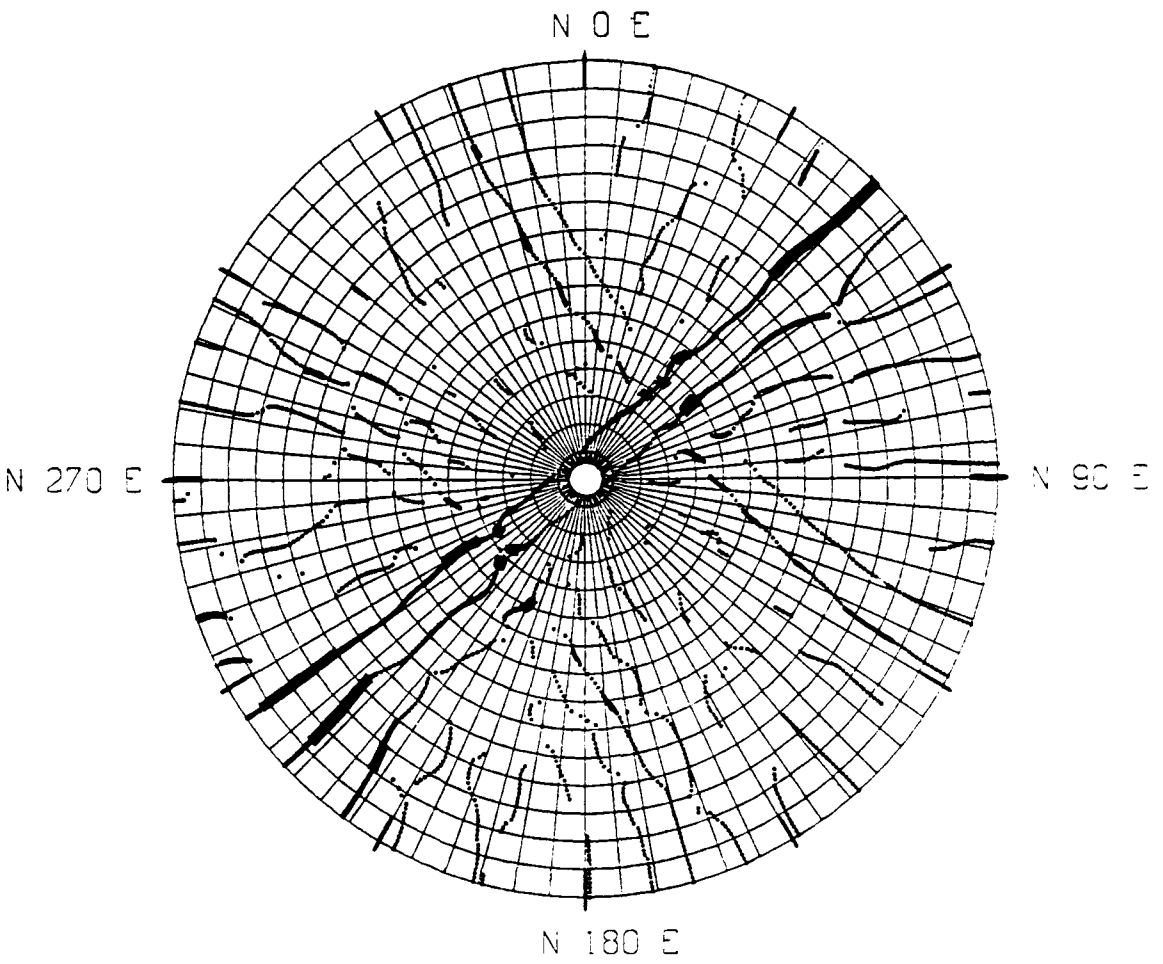

Figure 25. Sky plot of all peaks of TMUSIC for Nov. 25, 1977 at 10:30:20, scans 119-130. Legend: Thick line 0 to -15 dB, thin line -15 to -16.2 dB, dots -16.2 to -17.8 dB.

The MUSIC algorithm in the above cases was clearly able to identify a weaker source which had been missed by the DOPFUR analyses. Both analysis were carried out on ungroomed data, and for such data, signals which are more than 15 dB weaker than the strongest signal would probably be difficult to unambiguously identify using the TMUSIC program. Using groomed data, weaker sources could be identified using the MUSIC algorithm, but these could become lost in the grating and side-lobe structures of the stronger sources. The chirp analysis of Montbriand (1981) was capable of separating signals into different ranges so its overall amplitude range was some 40 dB. The weakest signals found in the chirp analysis would not be identified using the MUSIC algorithm because of the side-lobe structures. Much more work is needed to thoroughly investigate the potential of the MUSIC algorithm for separating closely spaced sources or sources with very different amplitudes.

10. Conclusions

A Peak Identification (PI) technique is presented which uses the FFT algorithm for unambiguously identifying up to three sources in signals received by the sampled aperture receiving array (SARA) of the Communications Research Centre. The technique is simple and fast and can be implemented with any array configuration.

The identification of the sources was found to be subject to the limitations of the FFT for resolving multiple sources in that there are certain combinations of amplitudes and phases that the sources could have that would prevent them from being identified. Equally important, there will be an inherent bias for secondary and tertiary sources to appear at the positions of the side lobes of the primary or strongest source. There appears to be a limit to the magnitude of a weaker source relative to that of the strongest source, below which it becomes too difficult to reliably identify other true sources. For the SARA array this ratio is near -10 dB.

Time equivalent data can be used to determine directional results for each scan of the receivers and based on a time history of such scans it is possible to determine the Doppler frequency of the different sources. This information can be used to verify the authenticity of some of the weaker sources identified.

Work had only been initiated on the potential of the MUSIC algorithm for determining accurate direction-of-arrival estimates of sources when this project was terminated. In the time available it became clear that the MUSIC algorithm is capable of resolving multiple sources not identifiable by the FFT technique by narrowing the main lobe and suppressing the side and grating lobes so that the largest of these lobes is some 10 dB below those obtained using the FFT algorithm. The MUSIC algorithm appears to be limited in the same way as the FFT algorithm in identifying very weak sources in that it too has a side lobe and grating lobe structure which will mask weak sources. Much more work is needed to investigate its full potential for processing signals received by the SARA array.

11. Acknowledgements

The author wishes to thank Dr. Eric Hung for the information present in Appendix A and for his consultation and advice on use of the MUSIC algorithm. A thanks is also extended to Dr. R. Jenkins for his constructive comments on this work. This work was sponsored by the Department of National Defence.

12. References

Martin, G.E., Signal Subspace Processing of Actual Radio and Acoustic Data, Report by Martin Analysis Software Technology, Inc., San Diego, Calif., 213pp., Feb. 1988.

Montbriand, L.E., The Dependence of Direction Finding Accuracy on Aperture Size, CRC Report No. 1343, June 1981.

Rice, D.W., Phase Characteristics of Ionospherically-Propagated Radio Waves, Nature Physical Science, Vol. 244, No. 136, pp.86-88, 6 Aug. 1973.

Rice D.W. and Winacott, E.L., A Sampling Array for the H.F. Direction Finding Research, 41pp, CRC Report No. 1310, October 1977.

Schmidt, R.O., A Signal Subspace Approach to Multiple Emitter Location and Spectral Estimation, 201pp., Ph. D. Dissertation of Stanford University, Nov. 1981.

Unpublished paper

Winacott, E.L., A Re-examination of High-frequency Direction-finding by Phase-front Testing. Presented at a Working Group Meeting held in Boston, Nov. 1986.

Personal Communication

Hung, E., 1986.

13. Appendix

MUSIC Algorithm Calculations

1. Let the vector bf **a** be a complex sample of the signals received at a particular instant by the M antennas of the receiving array. This "snapshot" is denoted as a column vector as $\mathbf{a} = (a_1^*, a_2^*, \ldots, a_M^*)^T$, where T denotes the transpose operator.

   Let $\mathbf{a_r}$ be the complex conjugate of the reverse sequence of **a**, where $\mathbf{a_r}=(a_M, a_{M-1}, \ldots, a_1)^T$. Note that the array elements must be evenly spaced, and if not, they must be symmetrically spaced so that the phases of the conjugate reverse sequence match those of the forward sequence.

2. For each snapshot calculate the covariance matrix **R** of **a** and sum for N snapshots.

$$R = 1/N \sum_{n=1}^{N} \mathbf{a_n a_n}^H$$

   where $\mathbf{a_n}^H$ is the Hermitian (conjugate transpose) of $\mathbf{a_n}$.

   Also calculate the covariance matrix of $\mathbf{a_r}$ and sum for N snapshots and add to the matrix for **a**.

Note: A superior solution is obtained by using the combined covariance matrix of the forward and reverse sequenced data. It was found by the author that for the theoretical data no satisfactory solution could be obtained using just the forward sequenced data a; one may have been possible if the theoretical data contained not only noise but adequate phase and amplitude 'jitter', but this still would have been inferior to that using the combined covariance matrix.

3. Determine eigenvalues and corresponding eigenvectors of the matrix evaluated in step 2.

4. Normalize each eigenvector to unity.

5. Order the eigenvalues in decreasing value and order the eigenvectors to correspond to the eigenvalues.

6. The signal space normally contains all eigenvalues within three to four orders of magnitude of the largest value. If these eigenvalues cannot be easily identified, the number of eigenvalues for the signal space should be at least a few more than the number of sources believed present in the recorded signal. It was found by the author that the precise number of eigenvalues for the signal space seemed to be less important than the inclusion of all of the eigenvalues of a group which had values which were all about the same.

   Let L be the number of eigenvectors identified for the signal space and let e_n be the n'th eigenvector of the signal space.

7. Assume the antenna array geometry is planar with antennas at positions x_i, y_i, $i=1,...,M$.

8. Assume a signal at an elevation angle Φ.

9. Assume the signal is at an azimuth Θ relative to a reference bearing, e.g. the x-axis.

10. The phase difference between phase fronts orthogonal to the line from the array centre to a source at the sky position (Θ, Φ) is $\delta_m = 2\pi d_m/\lambda$ or:

$$\delta_m = 2\pi (x_m \cos \Phi \cos \Theta + y_m \cos \Phi \sin \Theta)/\lambda$$

Calculate the column vector of the signal vector for the M antennas,

$$\mathbf{v}(\Theta) = (e^{j\delta_1}, e^{j\delta_2}..., e^{j\delta_M})^T/\sqrt{M}$$

11. Normalize v to unity.

12. Calculate ($\mathbf{v}(\Theta)\mathbf{v}^H(\Theta)$) and define as scalar p.

13. Calculate $\sum_{i=1}^{L} |e_i^H \mathbf{v}(\Theta)|^2$ and define as the scalar q.

14. The amplitude at the azimuth angle Θ is:

$$G(\Theta) = 1/(p - q)$$

15. Increment azimuth angle Θ and repeat steps 10 to 14.

16. Change to new elevation angle Φ and repeat steps 9 to 15.

17. Repeat steps 15 and 16 for the azimuths and elevations of interest.

18. Based on the $G(\Theta)$ distributions for the different Φ, identify sources and determine bearings, elevations and amplitudes.

DOCUMENT CONTROL DATA

(Security classification of title, body of abstract and indexing annotation must be entered when the overall document is classified)

1. ORIGINATOR (the name and address of the organization preparing the document. Organizations for whom the document was prepared, e.g. Establishment sponsoring a contractor's report, or tasking agency, are entered in section 8.)

DEPARTMENT OF COMMUNICATIONS
COMMUNICATIONS RESEARCH CENTRE
Box 11490, Station H, Ottawa, ON
K2N 8S2

2. SECURITY CLASSIFICATION (overall security classification of the document including special warning terms if applicable)

UNCLASSIFIED

3. TITLE (the complete document title as indicated on the title page. Its classification should be indicated by the appropriate abbreviation (S,C or U) in parentheses after the title.)

A Comparison of Direction Finding Results From an FFT Peak Identification Technique With Those From the Music Algorithm (U)

4. AUTHORS (Last name, first name, middle initial)

Montbriand, L. Edward

5. DATE OF PUBLICATION (month and year of publication of document)	6a. NO. OF PAGES (total containing information. Include Annexes, Appendices, etc.)	6b. NO. OF REFS (total cited in document)
July 1991	49	7

7. DESCRIPTIVE NOTES (the category of the document, e.g. technical report, technical note or memorandum. If appropriate, enter the type of report, e.g. interim, progress, summary, annual or final. Give the inclusive dates when a specific reporting period is covered.)

CRC Report #1438

8. SPONSORING ACTIVITY (the name of the department project office or laboratory sponsoring the research and development. Include the address.)

DEFENCE RESEARCH ESTABLISHMENT OTTAWA
SHIRLEY'S BAY
OTTAWA, ONTARIO K1A 0Z4

9a. PROJECT OR GRANT NO. (if appropriate, the applicable research and development project or grant number under which the document was written. Please specify whether project or grant)	9b. CONTRACT NO. (if appropriate, the applicable number under which the document was written)

10a. ORIGINATOR'S DOCUMENT NUMBER (the official document number by which the document is identified by the originating activity. This number must be unique to this document.)	10b. OTHER DOCUMENT NOS. (Any other numbers which may be assigned this document either by the originator or by the sponsor)
CRC REPORT #1438; 1410-041LA	

11. DOCUMENT AVAILABILITY (any limitations on further dissemination of the document, other than those imposed by security classification)

(X) Unlimited distribution
( ) Distribution limited to defence departments and defence contractors; further distribution only as approved
( ) Distribution limited to defence departments and Canadian defence contractors; further distribution only as approved
( ) Distribution limited to government departments and agencies; further distribution only as approved
( ) Distribution limited to defence departments; further distribution only as approved
( ) Other (please specify):

12. DOCUMENT ANNOUNCEMENT (any limitation to the bibliographic announcement of this document. This will normally correspond to the Document Availability (11). However, where further distribution (beyond the audience specified in 11) is possible, a wider announcement audience may be selected.)

UNCLASSIFIED

SECURITY CLASSIFICATION OF FORM

13. ABSTRACT (a brief and factual summary of the document. It may also appear elsewhere in the body of the document itself. It is highly desirable that the abstract of classified documents be unclassified. Each paragraph of the abstract shall begin with an indication of the security classification of the information in the paragraph (unless the document itself is unclassified) represented as (S), (C), or (U). It is not necessary to include here abstracts in both offical languages unless the text is bilingual).

A peak identification technique is presented which uses the FFT algorithm for unambiguously identifying up to three sources in signals received by the sampled aperture receiving array (SARA) of the Communications Research Centre. The technique involves (1) performing an FFT on a set of signals received by one of the two arms of the receiving array, (2) removing phase rotations resulting from the FFT and the data configuration, (3) interpreting this result as the direction cosine distribution of the received signal, (4) matching the locations and the amplitudes of all peaks with those in a master list for a single source, (5) repeating steps 1 to 4 with the second-arm data and (6) matching the phase and amplitude of potential sources on one arm to the phase and amplitude of potential sources on the other arm. The identification of the sources was found to be subject to the limitations of the FFT in that there was an inherent bias for the secondary and tertiary sources to appear at the side-lobe positions of the strongest source. There appears to be a limiting ratio of the magnitude of a weaker source to that of the strongest source, below which it becomes too difficult to reliably identify other true sources. Their main-lobe peaks fall between the side-lobe peaks of the strongest peaks, but also present are contributions from side lobes of other sources and from noise and interference. For the SARA array this ratio is near -10 dB.

Time equivalent data can be used to determine directional results for each scan of the receivers and based on a time history of such scans it is possible to determine the Doppler frequency of the different sources. This information can be used to verify the authenticity of some of the weaker sources identified.

Some of the data were also analyzed using the MUSIC algorithm. The MUSIC algorithm yields a narrower directional peak for the sources than the FFT. For the SARA array, using ungroomed data, the largest side and grating lobes that the MUSIC algorithm produces are some 10 dB below the largest side and grating lobes that are produced using the FFT algorithm. Consequently the source-separation problem is reduced relative to that encountered with the FFT algorithm, but is not eliminated. The MUSIC algorithm is not as simple to use and is much slower than conventional techniques, including the peak identification technique described above.

14. KEYWORDS, DESCRIPTORS or IDENTIFIERS (technically meaningful terms or short phrases that characterize a document and could be helpful in cataloguing the document. They should be selected so that no security classification is required. Identifiers, such as equipment model designation, trade name, military project code name, geographic location may also be included. If possible keywords should be selected from a published thesaurus, e.g. Thesaurus of Engineering and Scientific Terms (TEST) and that thesaurus-identified. If it is not possible to select indexing terms which are Unclassified, the classification of each should be indicated as with the title.)

DIRECTION FINDING
FFT
MUSIC ALGORITHM
COMPARISON
THEORETICAL
EXPERIMENTAL